

The IBEX-Lo Sensor

S.A. Fuselier · P. Bochslers · D. Chornay · G. Clark · G.B. Crew · G. Dunn · S. Ellis ·
T. Friedmann · H.O. Funsten · A.G. Ghielmetti · J. Googins · M.S. Granoff ·
J.W. Hamilton · J. Hanley · D. Heirtzler · E. Hertzberg · D. Isaac · B. King ·
U. Knauss · H. Kucharek · F. Kudirka · S. Livi · J. Lobell · S. Longworth ·
K. Mashburn · D.J. McComas · E. Möbius · A.S. Moore · T.E. Moore · R.J. Nemanich ·
J. Nolin · M. O'Neal · D. Piazza · L. Peterson · S.E. Pope · P. Rosmarynowski ·
L.A. Saul · J.R. Scherrer · J.A. Scheer · C. Schlemm · N.A. Schwadron · C. Tillier ·
S. Turco · J. Tyler · M. Vosbury · M. Wieser · P. Wurz · S. Zaffke

Received: 31 July 2008 / Accepted: 20 February 2009 / Published online: 9 May 2009
© Springer Science+Business Media B.V. 2009

S.A. Fuselier (✉) · A.G. Ghielmetti · J.W. Hamilton · E. Hertzberg · D. Isaac · A.S. Moore · C. Tillier
Lockheed Martin Advanced Technology Center, 3251 Hanover St, Palo Alto, CA 94304, USA
e-mail: stephen.a.fuselier@lmco.com

A.G. Ghielmetti
e-mail: gmetti@spasci.com

J.W. Hamilton
e-mail: Jon.Hamilton@lmco.com

E. Hertzberg
e-mail: Eric.Hertzberg@lmco.com

D. Isaac
e-mail: Donald.Isaac@lmco.com

C. Tillier
e-mail: Clemons.Tillier@lmco.com

G. Clark · S. Ellis · J. Googins · M.S. Granoff · D. Heirtzler · B. King · U. Knauss · H. Kucharek ·
F. Kudirka · S. Livi · S. Longworth · E. Möbius · J. Nolin · M. O'Neal · L. Peterson · S. Turco · J. Tyler ·
M. Vosbury · S. Zaffke
University of New Hampshire, 39 College Road, Morse Hall, Durham, NH 03824, USA

E. Möbius
e-mail: Eberhard.Moebius@unh.edu

P. Bochslers · D. Piazza · L.A. Saul · J.A. Scheer · P. Wurz
Physikalisches Institut, University of Bern, Sidlerstrasse 5, 3012 Bern, Switzerland

P. Wurz
e-mail: peter.wurz@phim.unibe.ch

G. Dunn · J. Hanley · D.J. McComas · S.E. Pope · J.R. Scherrer
Southwest Research Institute, 6220 Culebra Rd., San Antonio, TX 78238, USA

Abstract The IBEX-Lo sensor covers the low-energy heliospheric neutral atom spectrum from 0.01 to 2 keV. It shares significant energy overlap and an overall design philosophy with the IBEX-Hi sensor. Both sensors are large geometric factor, single pixel cameras that maximize the relatively weak heliospheric neutral signal while effectively eliminating ion, electron, and UV background sources. The IBEX-Lo sensor is divided into four major subsystems. The entrance subsystem includes an annular collimator that collimates neutrals to approximately $7^\circ \times 7^\circ$ in three 90° sectors and approximately $3.5^\circ \times 3.5^\circ$ in the fourth 90° sector (called the high angular resolution sector). A fraction of the interstellar neutrals and heliospheric neutrals that pass through the collimator are converted to negative ions in the ENA to ion conversion subsystem. The neutrals are converted on a high yield, inert, diamond-like carbon conversion surface. Negative ions from the conversion surface are accelerated into an electrostatic analyzer (ESA), which sets the energy passband for the sensor. Finally, negative ions exit the ESA, are post-accelerated to 16 kV, and then are analyzed in a time-of-flight (TOF) mass spectrometer. This triple-coincidence, TOF subsystem effectively rejects random background while maintaining high detection efficiency for negative ions. Mass analysis distinguishes heliospheric hydrogen from interstellar helium and oxygen. In normal sensor operations, eight energy steps are sampled on a 2-spin per energy

D. Chornay · J. Lobell · T.E. Moore · P. Rosmarynowski
Goddard Space Flight Center, Greenbelt, MD 20771, USA

T.E. Moore
e-mail: Thomas.e.moore@nasa.gov

M. Wieser
Swedish Institute of Space Physics, Box 812, 98128 Kiruna, Sweden
e-mail: wieser@irf.se

C. Schlemm
Applied Physics Laboratory, Johns Hopkins University, 11100 Johns Hopkins Road, Laurel, MD 20723,
USA
e-mail: chuck.schlemm@jhuapl.edu

K. Mashburn
Montana State University, Bozeman, MT, USA
e-mail: kmashburn@swri.edu

H.O. Funsten
ISR Division MS B241, Los Alamos National Laboratory, Los Alamos, NM 87535, USA

T. Friedmann
Sandia Laboratory, Mail Stop 1415, PO Box 5800, Albuquerque, NM 87185, USA
e-mail: tafried@sandia.gov

R.J. Nemanich
University of Arizona, Tuscon, AZ, USA

N.A. Schwadron
Boston University, 725 Commonwealth Ave, Boston, MA 02215, USA
e-mail: nathanas@bu.edu

G.B. Crew
MIT Kavli Institute for Astrophysics and Space Research, 77 Massachusetts Ave, Cambridge,
MA 02139, USA
e-mail: gbc@sapce.mit.edu

step cadence so that the full energy range is covered in 16 spacecraft spins. Each year in the spring and fall, the sensor is operated in a special interstellar oxygen and helium mode during part of the spacecraft spin. In the spring, this mode includes electrostatic shutoff of the low resolution ($7^\circ \times 7^\circ$) quadrants of the collimator so that the interstellar neutrals are detected with $3.5^\circ \times 3.5^\circ$ angular resolution. These high angular resolution data are combined with star positions determined from a dedicated star sensor to measure the relative flow difference between filtered and unfiltered interstellar oxygen. At the end of 6 months of operation, full sky maps of heliospheric neutral hydrogen from 0.01 to 2 keV in 8 energy steps are accumulated. These data, similar sky maps from IBEX-Hi, and the first observations of interstellar neutral oxygen will answer the four key science questions of the IBEX mission.

Keywords Neutral atom imaging · Heliosphere · Termination shock · Energetic neutral atoms · Magnetosphere · Surface ionization

Contents

1 Introduction and Basic Science	119
2 Basic Sensor Requirements	121
3 IBEX-Lo Sensor Subsystems	122
3.1 Introduction	122
3.2 Entrance Subsystem	123
3.3 ENA to Ion Conversion Subsystem	126
3.4 Energy Analysis Subsystem	129
3.5 Mass (TOF) Analysis Subsystem	131
3.6 TOF and Other Electronics	133
3.7 Star Sensor	134
3.8 Prototype Tests Prior to Sensor Development	135
3.9 Flight Sensor Calibration and Performance	136
3.10 Sensor Operation	143
3.11 Data Products	144
4 Summary	145
Acknowledgements	145
References	146

1 Introduction and Basic Science

The IBEX mission achieves its sole objective by answering four fundamental science questions that are described in detail in the IBEX mission overview and the IBEX science introduction (McComas et al. 2004, 2009). These four questions focus on the global interaction between the solar wind and the interstellar medium. They are:

Question 1: What is the global strength and structure of the termination shock?

Question 2: How are energetic protons accelerated at the termination shock?

Question 3: What are the global properties of the solar wind flow beyond the termination shock and in the heliotail?

Question 4: How does the interstellar flow interact with the heliosphere beyond the heliopause?

The science questions are answered using sky maps of heliospheric neutral fluxes from 10 eV to 6 keV and with observations of the interstellar neutral oxygen and helium flows. The sky maps are obtained from the combined IBEX science payload.

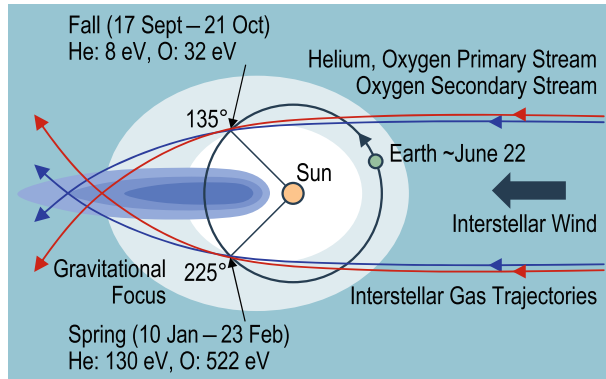
The IBEX payload consists of the IBEX-Hi and -Lo sensors and the Combined Electronics Unit (CEU). The payload is designed to operate as a single entity. Thus, there is little distinction between IBEX-Hi and IBEX-Lo sensor science objectives. Two neutral atom sensors are needed for the payload because interstellar and heliospheric neutrals span an energy range that is large enough to require two different detection techniques. In particular, techniques used to convert neutrals to ions (so that the ions can be accelerated and analyzed) change at energies around several hundred electron volts (Wurz 2000). This natural division in conversion techniques results in two sensors with significant energy overlap that provide independent measurements of heliospheric hydrogen neutrals over the entire energy range of interest.

The IBEX-Lo sensor measures the low-energy part of the heliospheric neutral spectrum. The energy range for this sensor is from 10 eV to 2000 eV. The lower bound of the energy range is set by sensor sensitivity and practical interpretation of the observations. A 10 eV neutral from the heliospheric termination shock requires almost 11 years to complete a trip from the shock to the inner heliosphere. Neutrals with energies less than 10 eV would take more than a solar cycle to complete the trip. In addition, the sensitivity decreases relatively rapidly below 10 eV because the neutral-to-ion conversion efficiency decreases at energies below 10–20 eV (see Sect. 3.3 and also see Wurz et al. 2006).

The upper bound of the energy range is set by electric fields in the sensor, voltages on the electrodes, and, ultimately, on sensor mass resources. In total, the IBEX-Lo energy range covers very low energy neutrals expected to survive the journey into the inner heliosphere, through nominal solar wind energy neutrals (and the expected energy peak in heliospheric neutral flux for some heliospheric interaction models) and into the energy range for suprathermal neutrals accelerated in the solar wind and at the heliospheric termination shock. Since the IBEX-Hi sensor measures down to ~ 300 eV and has very good sensitivity at ~ 1000 eV, there is significant energy overlap between the two sensors for important heliospheric measurements near the nominal solar wind energy of 1000 eV.

IBEX-Lo also provides measurements that are used to answer the fourth IBEX mission science question: How does the interstellar flow interact with the heliosphere beyond the heliopause? Because interstellar oxygen and helium neutrals have energies up to several hundred electron volts, contributions to this science question come primarily from the IBEX-Lo sensor. Figure 1 shows locations in the Earth's orbit plane where interstellar oxygen and helium will be measured and also shows predicted energies of the neutrals. The Earth is in the upwind direction in June. Each year in the "northern hemisphere fall" (135° from the upwind direction, with prime viewing from 17 Sept to 21 October), the Earth is moving in the same direction as interstellar neutrals from the upwind direction. Because interstellar neutrals are accelerated by the Sun's gravitational force, they have higher energies than when they first enter the solar system, but they have to "catch up" to the Earth. IBEX-Lo will observe oxygen at a center energy of only 32 eV and helium will be at 8 eV energy with respect to the Earth's motion. Thus, helium will be just below the sensor's 10 eV low energy cutoff. Each year in the "northern hemisphere winter/early spring" (hereafter referred to as "spring") (225° from the upwind direction, with prime viewing from about 10 January to 23 February), the Earth's velocity vector and the interstellar neutral velocity vector are directed nearly opposite one another, so neutrals have considerably higher energies. IBEX-Lo will observe oxygen at 522 eV and helium at 130 eV.

Fig. 1 Interstellar oxygen and helium observations occur in the fall and spring, where the streams intersect the Earth's orbit and the IBEX-Lo sensor FOV. In the fall, the interstellar neutral flux vector is in the same direction as the Earth's orbit velocity, so energies are low. In the spring, the two vectors are nearly oppositely directed, so energies are high



A key observable parameter for science question 4 is the arrival direction of the primary and secondary “filtered” neutral oxygen streams relative to the helium arrival direction. Measuring this arrival direction drives the IBEX-Lo sensor design in several ways discussed later in this paper.

2 Basic Sensor Requirements

Heliospheric and interstellar neutral fluxes are low and potential background contributions are very high. For comparison, 1000–2000 eV neutral fluxes from the Earth's magnetosphere (ring current) are $\sim 4 \times 10^4$ ENAs/(cm² s sr) and ~ 50 eV neutral fluxes from high latitude ionospheric outflow range from 6×10^4 to 1×10^6 ENAs/(cm² s sr). These neutral fluxes can vary significantly on timescales of tens of minutes. Magnetospheric and ionospheric neutrals are readily imaged with moderately large neutral atom imagers like the ones that were on the IMAGE spacecraft (Pollock et al. 2000; Moore et al. 2000; McComas et al. 2002; Fuselier et al. 2006). These imagers have time resolution of minutes, commensurate with the variability timescales of the source neutrals.

In contrast, ~ 1000 eV neutral fluxes from the outer heliosphere are predicted to range from 10^1 to 10^3 ENAs/(cm² s sr) and ~ 50 eV fluxes are predicted to range from 3×10^1 to 3×10^3 ENAs/(cm² s sr), depending on several factors including the termination shock strength (Gruntman et al. 2001). Recent measurements of energetic neutral atoms from the heliosheath suggest that these estimates may be somewhat low (Galli et al. 2006; Wurz et al. 2008b). However, heliospheric neutral fluxes are still considerably lower than magnetospheric ENA fluxes.

Variability timescales for ENAs from the outer heliosphere are not known. However, propagation times for neutrals from the vicinity of the termination shock to the inner solar system range from months (for ~ 1 keV ENAs) to years (for ~ 50 eV ENAs). ENAs from the termination shock propagating into the inner heliosphere have a 10–20% probability of charge exchange with solar wind protons, (i.e., only 80–90% of the original ENA signal can be detected at Earth orbit). This charge exchange is localized within the last 10 AU. However, if the ENA path goes through the plasma of a coronal mass ejection (CME), where there can be significantly higher proton densities, complete extinction of the ENA signal is possible. Given the typical CME frequencies with respect to propagation times of the ENAs, signal fluctuations at timescales of the order of days are possible.

Thus, compared to magnetospheric neutral fluxes, heliospheric neutral fluxes are from 10 to more than 1000 times lower, but the required time resolution for the observations is

much longer. The very low fluxes and long timescales drive the IBEX sensor design away from imaging systems (like those used on the IMAGE mission) and to a large geometric factor, single pixel camera. Full energy and angle images with appropriate time resolution are accumulated by reorienting the (spinning) IBEX spacecraft over the course of 6 months, as described in the mission overview (McComas et al. 2009).

Potentially high contributions from background ions and UV also drive sensor design. For magnetospheric imagers, one can use a large geometric factor, pinhole camera (e.g., Pollock et al. 2000) for imaging because the signal to noise ratio is relatively large. This technique of direct detection of neutrals is not possible for the IBEX mission because creation of ions within the sensor from, for example, UV background could overwhelm the heliospheric signal. Furthermore, for IBEX-Lo, heliospheric neutrals have too low an energy to be directly detected with any reasonable efficiency (Wurz 2000). These background considerations and detection efficiencies drive the overall sensor design away from a direct detection, pinhole camera concept. Instead, heliospheric neutrals are ionized in the sensor and resulting ions are accelerated (to improve detection efficiency) and deflected away from their incident trajectory (to separate signal ions from potential backgrounds such as UV). Finally, coincidence measurements are used because this technique combines high detection efficiency with very high background rejection.

High throughput of the relatively weak heliospheric signal and very good background rejection are key elements in each of the IBEX-Lo sensor subsystems. In the next section, the sensor and these subsystems are described, with emphasis on contributions each subsystem makes to the overall signal detection and background rejection.

3 IBEX-Lo Sensor Subsystems

3.1 Introduction

The IBEX-Lo sensor is a large geometric factor, single pixel camera. It uses a large annular entrance to collimate the neutral flux. This entrance has positive and negative electrodes that reject incoming ions and electrons. The neutrals pass through the collimator and strike a conversion surface at a shallow angle (nominally 15°) where a fraction of them are converted to negative ions. These negative ions are accelerated in an electrostatic analyzer (ESA) that also selects the sensor energy range and resolution. Upon exiting the ESA, negative ions are further accelerated into a multiple carbon foil time-of-flight (TOF) mass spectrometer that measures ion mass.

Figure 2 shows a cross-section of the sensor (rotationally symmetric about the centerline of the figure with a maximum radius of about 15 cm). Major components are labeled on the right hand side, and representative trajectories of neutrals, ions, and electrons, are shown on the left hand side. A picture of the front entrance of the sensor (in the calibration vacuum chamber) with some of the components labeled is shown in Fig. 3. Table 1 shows a summary of the sensor parameters and resources.

The sensor consists of four major subsystems: the entrance, ENA to ion conversion, energy analysis, and mass (TOF) analysis subsystems. These four subsystems are attached to the “optics deck”, which provides the stable mechanical platform for the ion optics and also a stable connection to the IBEX spacecraft. The four subsystems operate together, maximizing sensitivity and minimizing background to produce the highest possible signal to noise measurements over the IBEX-Lo energy range.

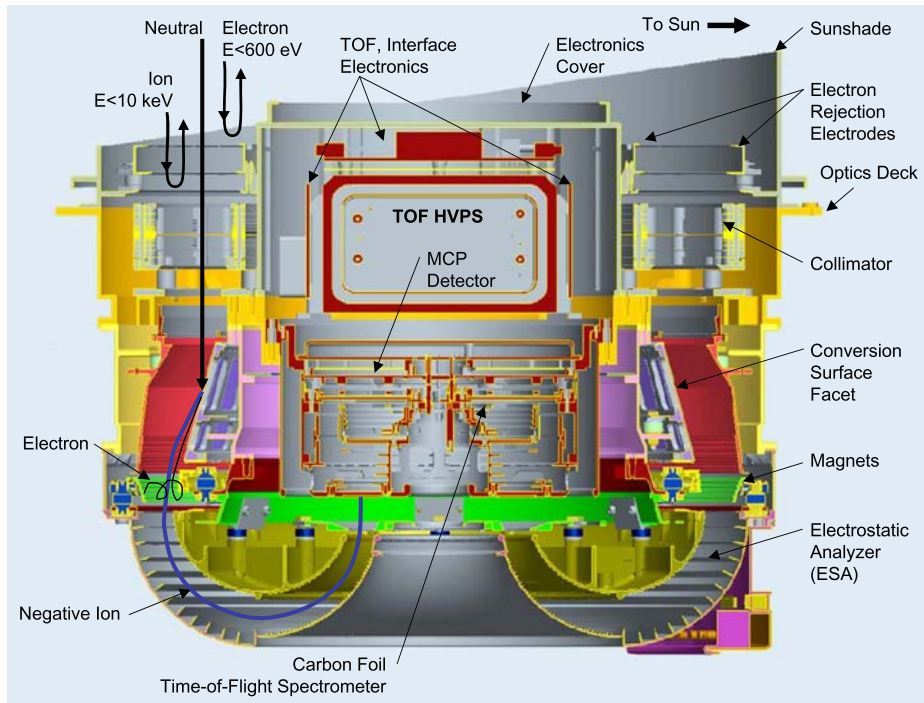


Fig. 2 Cross-section of the IBEX-Lo sensor showing the primary components. The sensor is rotationally symmetric about the centerline axis of the figure. Electrons, neutrals, and ions all enter the sensor through the collimator. Charged particles are rejected by the collimator and electron rejection electrodes. Neutrals pass through the collimator and strike a conversion surface. A fraction of these incident neutrals leave the conversion surface as negative ions and pass through the electrostatic analyzer. Electrons from the conversion surface are deflected by two concentric rings of permanent magnets. Negative ions exit the ESA, are accelerated and enter a triple coincidence time-of-flight (TOF) mass spectrometer. In this subsystem, the ion mass is determined

3.2 Entrance Subsystem

The entrance subsystem consists of the sunshade, electron rejection electrodes, and collimator. The sunshade is cut at an angle so that sunlight cannot reflect off any part of the sensor onto the collimator. Eliminating scattered sunlight from the collimator entrance is critical for background reduction. The sensor views 90° away from the spacecraft spin axis and the spin axis is reoriented towards the Sun every orbit (8 days). By setting the spin vector a few degrees off the Sun and letting it precess through the Sun direction, the spin vector will move a maximum of about $\pm 4^\circ$ off the Sun direction over the course of an orbit. Thus, with margin, the sunshade was designed to block sunlight for a spin axis that is up to 8° off of the Sun direction. Elimination of sunlight reduces UV flux into the sensor to interstellar levels (~ 800 Rayleighs maximum flux at Lyman Alpha wavelength) during prime science observations. The UV flux will be considerably greater (~ 20 kRayleighs at Lyman Alpha wavelength) when the sensor views the Earth (twice per year), but, at those times, the sensor will be viewing through the Earth's magnetosphere and not making prime heliospheric science measurements.

Since the sensor views 90° from the Sun direction, the cold (temperatures of ~ 10 's of eV maximum), flowing (~ 400 km/s away from the Sun) solar wind ion distribution does

Fig. 3 Photograph of the IBEX-Lo sensor entrance system in the calibration vacuum chamber. The star sensor is at the bottom and, in this orientation, the Sun direction is up. The collimator is divided into 4 quadrants by thin spokes located at 0° , 90° , 180° , and 270° relative to the Sun direction. In the lower left hand quadrant, the hexagon pattern that defined the FOV is smaller than the one in the other three quadrants. This high resolution sector is used to determine the flow direction of the interstellar neutral oxygen during the spring observing period

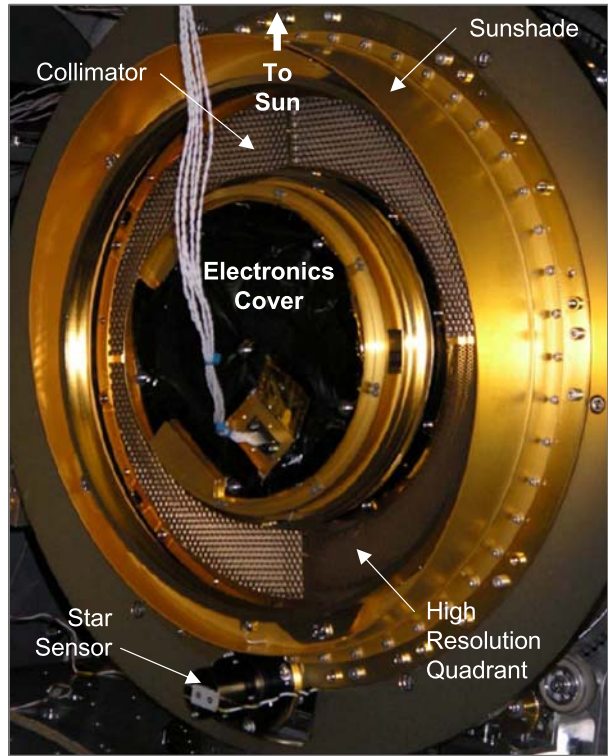


Table 1 IBEX-Lo sensor parameters and resources

Energy Range (eV)	10–2000
Energy resolution ($\Delta E/E$)	0.8
Mass Range	1–32 amu
Mass Resolution $M/\Delta M$	> 4
Field of View—Low Resolution	$6.54^\circ \times 6.54^\circ$
Field of View—High Resolution	$3.19^\circ \times 3.19^\circ$
Geometric Factor* ($\text{cm}^2 \text{sr}$)	0.91
Mass (kg)	11.5
Power (W)	3.46
Telemetry (bps)	122

*This geometric factor refers only to the collimator opening and is the sum of the high and low resolution sectors, not including grid transmission factors, neutral-to-ion conversion efficiencies, ESA or TOF efficiencies

not have direct access to the sensor through the collimator. However, the solar wind (halo) electron distribution has sufficient temperature that a significant electron flux in the energy range from 10's to 100's of eV could enter the sensor. These electrons could ionize residual gas inside the sensor through electron impact ionization. The newly created ions would be accelerated into the conversion surface, and resulting negative ions would be indistinguishable from those created by source heliospheric neutrals. To eliminate low-energy electrons, a pair of electron rejection electrodes encircles the entrance to the collimator. The electrodes are charged to -3.1 kV , creating a field that rejects up to 600 eV electrons from the collimator.

The collimator defines the instantaneous fields-of-view (FOVs) of the sensor and is held at a positive high voltage of 10 kV to keep energetic, positive ions (up to 10 keV) out of the sensor. The collimator designs for IBEX-Hi and -Lo are identical except that the annular diameter of the IBEX-Lo collimator is smaller and the IBEX-Lo collimator has two separate FOVs. The two FOVs are a high (angular) resolution FOV (one 90° azimuthal quadrant) and a low resolution FOV (three 90° azimuthal quadrants). The high resolution FOV has approximately one fourth the intrinsic angular FOV of the low resolution quadrant and is used to measure interstellar neutral oxygen in the springtime (see Fig. 1). The full sensor (combined high and low resolution FOVs) is used for heliospheric neutral hydrogen measurements throughout the year and for measurements of interstellar neutral oxygen in the fall.

To provide a well-defined angular FOV with the largest possible collection area for neutral atoms, the collimator has a hexagon shape multi-hole aperture that uses a stack of identical photo-etched plates. A linear version of this type of collimator was used on the ACE/SEPICA instrument (Möbius et al. 1998a).

Figure 3 shows the front of the collimator hexagon pattern. The collimator is divided into four 90° quadrants by 4 spokes at approximately 0°, 90°, 180°, and 270° from the vertical (Sun) direction. The high-resolution quadrant is between the 90° and 180° spokes measured clockwise from vertical in Fig. 3. Optical tests of the IBEX-Lo collimator show that the full-width half-max (FWHM) FOV of the low resolution quadrants is $6.54^\circ \pm 0.23^\circ$ and the FWHM FOV of the high resolution quadrant is $3.19^\circ \pm 0.2^\circ$, or very close to the designed low- and high-resolution FOVs of $7^\circ \times 7^\circ$ and $3.5^\circ \times 3.5^\circ$, respectively.

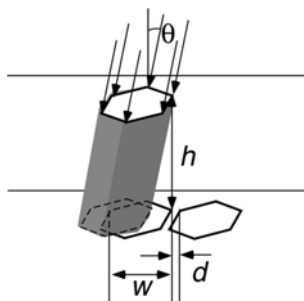
The FOV is determined solely by the width w (~ 4 mm for the low resolution sectors) of the hexagon openings and the total height h (~ 25.9 mm) of the collimator stack, i.e., between the entry and exit plate, as shown in Fig. 4. The angular width of the FOV in each direction is calculated from progressive clipping of trajectories through the aperture pair as the angle θ relative to the normal direction of the collimator plates increases. The maximum throughput is at normal incidence and is determined by the transparency T of the collimator. The transparency is dependent solely on the ratio of the line width d and the width of the hexagons w , and is written as:

$$T = 1/(1 + d/w)^2. \tag{1}$$

The collimator has a transmission of $68.8 \pm 0.3\%$ for the low resolution quadrants and $61.7 \pm 0.5\%$ for the high resolution quadrant.

In Fig. 4, particles can pass through neighboring channels in a multi-hole collimator as long as their angle θ exceeds $\theta \geq d/h$. To prevent such “leakage” of particle trajectories, identical collimator plates are stacked in a roughly geometric sequence, with the largest plate separation $h_n \leq d \cdot h/w$ and the smallest separation so that $h_1 \leq d \cdot \tan \theta_{\text{Max}}$, where

Fig. 4 Pair of entry and exit aperture holes of the IBEX-Lo collimator. As indicated by the shaded hexagon shape, only the fraction of particles pass the collimator that fall into the intersection of the two hexagon areas at the exit plate. The fraction depends on the distance h between the plates, the opening width w , and the separation d between hexagons



θ_{Max} is the largest possible incidence angle for particles. The angle θ_{Max} is limited to $\leq 50^\circ$ by a precision-milled pre-collimator with trapezoid-shaped hexagon ribs, whose width is $\geq 50 \mu\text{m}$ less than d . The geometric sequence of plate separations starts with the largest one at the exit plate and alternates to smaller and smaller separations from both the top and bottom toward the center so that a series of 6 plates with the smallest identical separations is placed at the center of the collimator. With this pattern, the fraction of particles scattered at the edges of the holes into the FOV (an unavoidable effect) is minimized. Very thin (0.5 mm thick) etched plates with sharp edges are also used to reduce the scattered particle fraction. Finally, plate separations are reduced compared to a strictly geometric progression to account for manufacturing tolerances and deviations from planarity in the collimator plates.

Accounting for collimator transmission, correcting for losses due to spokes, incomplete hexagons at the edges, and shadowing at the edges, and combining the FOVs of 3 low resolution quadrants and one high resolution quadrant, the total geometric factor of the collimator is $0.91 \pm 0.04 \text{ cm}^2 \text{ sr}$.

The collimator floats at +10 kV relative to the spacecraft (and sensor) ground potential and is attached to the optics deck by 16 high voltage insulators. This positive potential keeps up to 10 kV ions out of the sensor. While nominal solar wind ion fluxes directed into the sensor with energies above a few 10^3 's of eV are very low, energetic ion fluxes (up to several keV) in the magnetosheath and in the Earth's foreshock upstream from the bow shock can be high enough to create measureable background in the sensor. The positively biased collimator rejects these ions.

Without the +10 kV collimator voltage, the IBEX-Lo design provides some mitigation against ion background. First, the negative electrodes in front of the collimator act as a defocusing lens for low energy ions. Simulations show that ions below about 200 eV are defocused enough that they hit the collimator plates before entering the sensor. Second, there is a conical-shaped grid between the collimator and the ENA to ion conversion subsystem (described in Sect. 3.3 below) that deflects ions away from the conversion surface. Finally, IBEX-Lo is inherently a negative ion sensor. Any positive ion that enters the sensor must be converted to a negative ion on the conversion surface in order to be detected as background.

3.3 ENA to Ion Conversion Subsystem

By rejecting the majority of high energy ions and nearly all electrons, only UV, a very low flux of solar wind energetic ions with energies $> 10 \text{ keV}$, and neutrals exit the back of the collimator. These constituents enter the subsystem where a fraction of the neutrals are converted to negative ions. The key to this subsystem is a diamond-like carbon (DLC), or more accurately described as a tetrahedral amorphous carbon (ta-C), conversion surface (e.g., Wieser et al. 2005).

As stated in the introduction, 10 eV to several hundred eV neutrals do not have sufficient energy to be detected directly with any efficiency using standard detector technology. Furthermore, heliospheric neutrals are accompanied by interstellar UV fluxes that would overwhelm a detector placed directly behind the IBEX-Lo collimator. Thus, neutrals must be converted to ions so that they can be accelerated (thereby raising their detection efficiency) and deflected away from the direct path taken by UV background (Wurz 2000; Wurz et al. 2006).

Ionization by scattering from charge-state conversion surface offers the highest ionization efficiencies in the energy range below 1 keV. This technique was first proposed for

space applications by Gruntman (1993) and Wurz et al. (1993). Early low energy neutral atom imager designs were proposed using low work function surfaces for converting neutrals to ions during surface impact and reflection (e.g., Ghielmetti et al. 1994). However, these surfaces must be re-conditioned and regenerated often, placing difficult requirements on sensor resources and operations. Furthermore, changing surface conditions result in variable conversion efficiencies and ultimately result in uncertainties in overall sensitivity of the sensor. This uncertainty creates the need for a separate, accurate monitor of conversion efficiency.

Since these early designs, there has been a concerted search for a stable, inert, high-yield, low-scatter conversion surface. The Low Energy Neutral Atom (LENA) imager on the IMAGE mission was the first to use this type of surface conversion. A highly polished polycrystalline tungsten surface was used for neutral to ion conversion, with ionization facilitated by natural contaminants, most likely adsorbed water (Moore et al. 2000). Surface conversion efficiencies were $\ll 1\%$ for hydrogen.

Since this pioneering mission, several surfaces have been identified that have better negative ion yield. Among these, natural diamond crystals demonstrated reasonably high negative ion production for hydrogen and oxygen (Wurz et al. 1997). The large conversion surface area required for most neutral atom imagers makes the use of natural diamond surfaces impractical from a cost standpoint. Instead, diamond-like carbon surfaces make an excellent substitute (Scheer et al., 2005, 2006; Wieser et al. 2005; Wurz et al. 2006). These diamond-like carbon surfaces are readily grown on large, very smooth silicon substrates, retaining the surface smoothness of the underlying substrate.

For IBEX-Lo, 3 inch silicon wafers were cut into trapezoidal facets 62 mm long and ~ 30 mm wide at the center. The edges of the trapezoids were beveled so that they fit together to form an annular cone that is inclined at 15° from the incident direction of the neutrals that pass straight through the collimator. A 100 nm thick tetrahedral amorphous carbon (ta-C) layer was grown on each trapezoid facet. At the start of this process, the silicon surface smoothness was < 0.1 nm RMS and, at the end, the DLC layer had surface smoothness ~ 0.1 nm RMS. These surfaces were then treated with a hydrogen beam in a vacuum. This process, called hydrogen termination, is used to chemically terminate exposed, non-diamond-like carbon bonds on the surface. It removes oxygen from the surface, making it more inert, and it also lowers the work function of the surface and does not add to surface roughness.

The end result was 28 facets that are inert, slightly conductive, extremely smooth, and have reasonably high negative ion yield for neutral impact at grazing (15°) incidence. A picture of one of the facets is shown in Fig. 5. The negative ion yield properties for hydrogen are shown in Fig. 6. Ionization efficiencies increase with increasing energy, reaching $\sim 5\%$ for hydrogen. Measurements of 4 of the facets are shown at 4 different energies. The empirical curve is based on measurements over the entire energy range using a variety of conversion surfaces and detectors (Wieser 2005; Wurz et al. 1998, 2006; Wieser et al. 2007). Tests of these surfaces over periods of more than several years indicate that the conversion efficiency is stable for many years (Scheer et al. 2005, 2006).

While Fig. 6 shows relatively high ionization efficiencies for the conversion surfaces, the conversion efficiency is the product of the ionization efficiency and the reflection efficiency. That is, the total negative ion yield is the ratio of the number of negative ions off the surface divided by the number of neutral atoms incident on the surface. The reflection efficiency plays an important role in determining the overall conversion efficiency for these diamond-like surfaces. The reflection efficiency is also energy and mass dependent (Scheer et al. 2008). The reflection efficiency is the number of scattered particles (atoms and negative

Fig. 5 Photograph of a conversion surface facet. The substrate is a highly polished silicon wafer cut into a trapezoid. A ~ 100 nm diamond surface is grown on this surface. The resulting conversion surface is smooth to within ~ 0.1 nm. Twenty eight of these facets are used in a conical configuration in the sensor

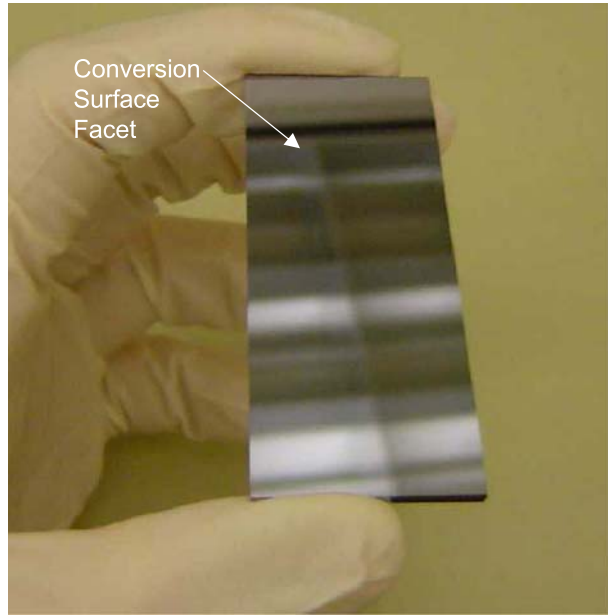
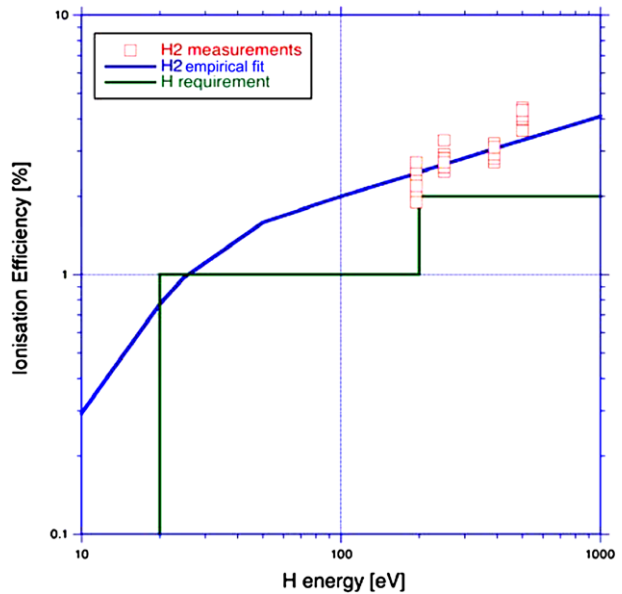


Fig. 6 Measured neutral to negative ion ionization efficiencies of IBEX-Lo conversion surfaces for hydrogen. The *green line* indicates the sensor requirement and the blue line is an empirical fit to measurements from different synthetic diamond coatings on silicon (Wieser 2005). The conversion efficiency is the product of these ionization efficiencies times the (energy dependent) reflection efficiencies



ions) in the specular direction within the ion-optical acceptance angle of the ion optical system. The roughness of the surface determines the fraction of negative ions that scatter in the specular direction. The IBEX-Lo conversion surfaces are smooth on an atomic level, maximizing this fraction of scattered negative ions. However, even these surfaces are corrugated at an atomic level. Therefore, there is always angular scatter away from the specular direction. The number of particles that scatter away from the specular direction increases with

particle energy and with angle of incidence because the incoming particles probe deeper into the surface potential well of the conversion surface. Thus, the reflection efficiency decreases with particle energy, since the angular scatter increases (Wahlström et al. 2008), and a lower fraction of the angular scatter width is within the angular acceptance of the ion optical system. In addition to this effect, there is the possibility that incoming particles get stuck in the surface.

Tests using the University of Bern's conversion surface test facility (Wurz et al. 1997; Jans et al. 2000) show that the reflection efficiency for the IBEX-Lo DLC surfaces is of the order of 10% for 200 eV hydrogen and of the order of 4% for 700 eV hydrogen (Scheer et al. 2008). Combined with the ionization efficiency (Fig. 6), these tests result in an overall conversion efficiency for hydrogen neutrals that is $< 1\%$ over the IBEX-Lo energy range. However, the IBEX-Lo sensor has ion optics that are designed to maximize capture of reflected negative ions, even some ions that scatter away from the specular direction, so the DLC surfaces in the sensor have measured conversion efficiencies that approach 1% at the upper energy limit. While this efficiency seems low, it is still one of the highest for inert conversion surfaces like the DLC surface.

Finally, ionization and reflection efficiencies also depend on incidence particle type. Ionization efficiencies are a strong function of the electron affinity of the incident neutral. Oxygen has a higher electron affinity than hydrogen and a much higher negative ion yield ($\sim 30\%$ compared to $\sim 5\%$ for hydrogen). Reflection efficiency is also dependent on mass. Tests conducted at the University of Bern's conversion surface test facility indicate that oxygen has, on average, a lower reflection efficiency than hydrogen. Also, the energy loss upon reflection is greater for oxygen than for hydrogen. Differences in the reflection efficiency and energy loss between oxygen and hydrogen are probably associated with the fact that hydrogen is much lighter than carbon (the conversion surface material) while oxygen and carbon have similar masses. The details of this interaction are still the subject of investigation (Wahlström et al. 2008).

3.4 Energy Analysis Subsystem

Negative ions from the conversion surface facets are accelerated away because the facets are held at a negative potential. Another electrode that faces the annular ring of conversion surface facets is also at a negative potential. In combination, these fields deflect and focus negative ions in the radial direction into the entrance of the Electrostatic Analyzer (ESA) (see the negative ion trajectory in Fig. 2). Large angle scattering off the conversion surface facets in this direction is at least partially compensated for by this focusing effect.

The energy analysis subsystem consists of a toroidal electrostatic analyzer (ESA), two electrodes at the entrance to the ESA that help deflect and focus the negative ions into the ESA, and a third electrode at the ESA exit that helps focus the negative ion beam into the mass analysis subsystem.

The toroidal ESA defines the sensor energy pass band. The analyzer has the shape of a "bundt" baking pan (Moestue 1973), and this geometry was used in the Toroidal Imaging Mass Angle Spectrograph (TIMAS) on the Polar spacecraft (Shelley et al. 1995). Parameters were adjusted so that the annular ring at the ESA exit was the same size as a standard size microchannel plate in the TOF spectrometer. Also, the plate separation between the inner and outer ESA is quite large (see Fig. 2), commensurate with the large passband of the sensor (the ESA $\Delta E/E$ is estimated to be 0.67). With such a large plate separation, there could be considerable UV background. To reduce the background, the ESA outer shell

has very large “fins” that are very effective light traps (see Fig. 2). In addition, the inner ESA shell is serrated and both the inner and outer shells were blackened with a porous black coating that further reduces UV reflection. These measures counteract the effect of the large plate gap and maintain an overall approximately 3-bounce system for UV to reach the entrance to the TOF system. Before the design of the IBEX-Lo sensor, a prototype sensor was built and all ion-optical properties were verified (Wieser 2005; Wieser et al. 2007) (see also Sect. 3.8).

In addition to setting the energy passband of the sensor, the ESA folds the ion optics so a smaller, standard size detector can be used. This reduction does not come without a price. Two fundamental ion optics properties of the ESA are that it focuses in the radial direction, but it disperses in the azimuthal direction. A narrow-angle beam entering the collimator at one point will disperse into an arc that is greater than $\sim 180^\circ$ in azimuthal extent at the detector. Since it is not necessary to image in the azimuthal direction, this dispersive property is not an issue for IBEX-Lo. However, ions that disperse to large azimuthal angles will exit the ESA at a very large angle with respect to the normal angle of the TOF entrance. The sensor properties at the ESA exit are designed to help deflect the azimuthal trajectories of negative ions so the ions arrive at the TOF entrance with a small angle relative to the normal. This deflection is done in two ways: by shaping the ESA exit so that it focuses ions and by applying a large acceleration voltage between the ESA exit and the TOF entrance. However, ions with very large azimuthal trajectories exit the ESA with too large an angle from the radial direction. These ions do not pass completely through the TOF system and are lost.

This fundamental property of the ESA feeds back to conversion surface smoothness. If negative ions leave the conversion surface with more than 10° azimuthal angle relative to their incident direction, then their trajectories in the ESA become large spirals and they exit the ESA at very oblique angles with respect to the normal to the TOF entrance and are lost. These ions are lost in the TOF system. Tests of the IBEX-Lo conversion surface facets indicates that they are smooth to $\sim 0.1\text{--}0.2$ nm RMS. Nonetheless, a significant fraction of the ions are lost in this manner and that fraction is energy dependent.

In addition to negative ions, incident neutrals produce electrons from the conversion surface. In fact, many more electrons are produced than negative ions because UV photons also reach the conversion surface. Since the ESA and energy analysis system are designed to accelerate negative ions, electrons could become a serious background in the TOF subsystem. Specifically, if a sufficient number of electrons are accelerated through the ESA and hit the first carbon foil in the TOF system, then they could overwhelm the TOF electronics.

To counter this background, the sensor takes advantage of the azimuthal defocusing property of the ESA. The energy analysis subsystem uses permanent magnets to deflect the electron trajectories so they have a large azimuthal component to their velocities. This electron suppression scheme was used effectively on the IMAGE/LENA imager (Moore et al. 2000) and tested in the IBEX-Lo prototype (Wieser et al. 2007) (see Sect. 3.8). For IMAGE/LENA, the electrons were suppressed after they were accelerated to several keV in the ion optics, and relatively large permanent magnets were needed (Moore et al. 2000). For IBEX-Lo, it was possible to design a magnetic suppression system for the electrons before they were accelerated significantly (electrons leaving the conversion surface have only a few eV energy) (Wieser et al. 2007). Furthermore, instead of deflecting the electrons so that they cannot enter the ESA, all that was required was to add a large azimuthal component to their velocities. Two nearly concentric circles of permanent magnets were used on the inner and outer electrodes that define the entrance to the ESA (see Fig. 2). These magnets (~ 1.5 mm in diameter) face each other across the ESA entrance gap and create a 3 millitesla field directed

radially across the gap. Electrons up to a few 10's of eV are effectively deflected in this field and, if they enter the ESA, their trajectories have significant azimuthal components, and therefore they do not reach the TOF entrance. The magnetic field is low enough that trajectories of even the lowest energy negative ions are unaffected.

Finally, the energy analysis subsystem has one more requirement. As discussed in Sect. 3.2 (the entrance subsystem), one of the four quadrants of the collimator has a high resolution, $3.2^\circ \times 3.2^\circ$ FOV. For interstellar neutral oxygen measurements in the spring-time, this quadrant must be used and the other three quadrants must be “shut off”. Shutoff is achieved electrostatically by applying a large, negative voltage (-2.5 kV) to the inner electrode at the entrance to the ESA for the three quadrants behind the low resolution collimator quadrants. This potential pushes negative ions in the three low resolution quadrants to the outer wall, where they scatter and do not enter the ESA. Tests of the IBEX-Lo sensor demonstrate that this shutoff works very well. The edges of the high resolution sector were of particular concern since fringe fields could affect ion trajectories in the low resolution sector and possibly allow “leakage” of these ions from low resolution sectors to the detector. Field termination electrodes are used to minimize fringe fields and therefore minimize leakage. Tests indicate that leakage is $< 1.5\%$ and, at this level, leakage does not affect high angular resolution measurements.

3.5 Mass (TOF) Analysis Subsystem

The mass (time-of-flight, TOF) analysis subsystem is a triple coincidence carbon foil-based time-of-flight ion mass spectrometer. It is designed to distinguish hydrogen and oxygen negative ions and suppress background random events through triple coincidence measurements. While distinguishing hydrogen and oxygen is the minimum mass resolution that is required, the TOF is designed with the goal to distinguish hydrogen and helium negative ions so that interstellar neutral helium fluxes can be measured separate from the interstellar neutral oxygen. This type of double and triple coincidence TOF system is a novel design that is based on the TOF systems used on FAST, Cluster, Equator-S, and STEREO/PLASTIC (e.g., Möbius et al. 1998b). The triple TOF system has several major advantages over previous designs. Advantages such as the superior background suppression and higher efficiency when single TOF channels are used are important for the IBEX-Lo sensor (Möbius et al. 2007).

The basic TOF operation is shown in Fig. 7. This figure shows a radial cross-sectional cut of the TOF subsystem. It is rotationally symmetric about the left hand side of the figure, so that the microchannel plate (MCP) detector stack (pink in the Fig. 7) is an annular ring. The section of the TOF in Fig. 7 is shown in the inverse orientation compared to Fig. 2. A picture of the entrance end of the flight model of the TOF is shown in Fig. 8. The eight carbon foils that make up the first set are supported on grids that are seen through the ultra-thin foils. Vent holes surround the foils to protect them from perforation by acoustic shock.

Negative ions are accelerated into the first set of foils at the top of Fig. 7 because the entire TOF ion optics section floats at a nominal $+16$ kV post-acceleration (PAC) high voltage. (The blackened ground cylinder that surrounds the optics is shown in Fig. 8). As discussed in Sect. 3.4, this high post acceleration voltage helps straighten out negative ion trajectories between the ESA exit and TOF entrance foils. More importantly, high post acceleration allows a TOF measurement with high enough resolution after energy loss in the entrance foil.

Upon striking the first set of carbon foils, negative ions knock off secondary electrons. These secondary electrons are focused on the outmost radius of the MCP and constitute the first start pulse (start 1 or “a” in Fig. 7). As the negative ions pass through the first

Fig. 7 Schematic of the TOF mass spectrometer. The TOF is rotationally symmetric about the right hand side of the figure. Negative ions from the ESA strike the first foil at the top. These ions pass through the foil (some become neutral) and knock off electrons that are accelerated and steered to the outer edge of the annular microchannel plate stack. The signal from these ions (a, on the anode below the pink MCP stack) is the start 1 signal. Ions and neutrals pass through a second, interior foil. Electrons from this foil are accelerated to the inner edge of the MCP stack and create the start 2 signal. Finally, ions and neutrals strike the MCP stack at position b0/b3 and create the stop signal. By combining the starts and stops, the mass of the incident negative ion is determined

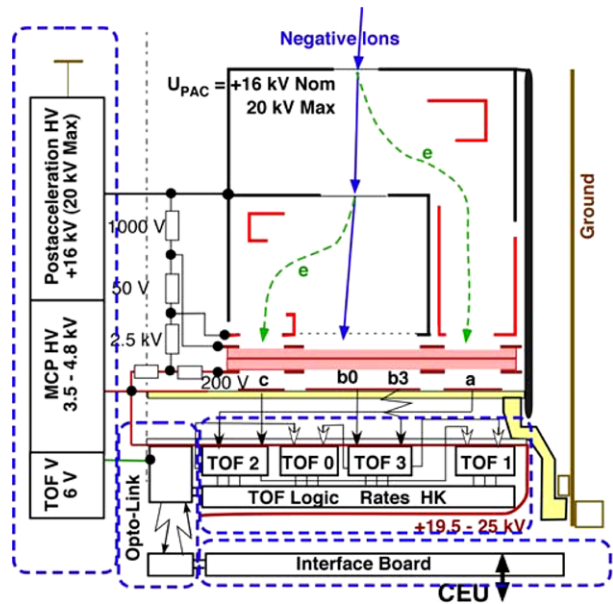
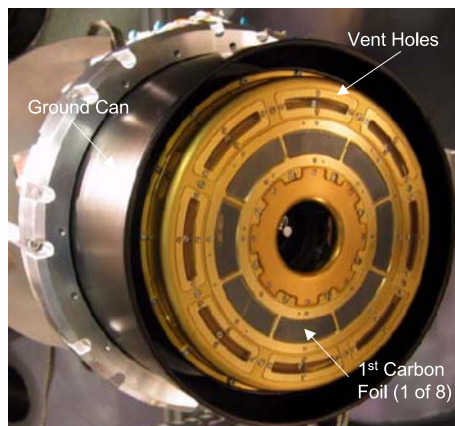
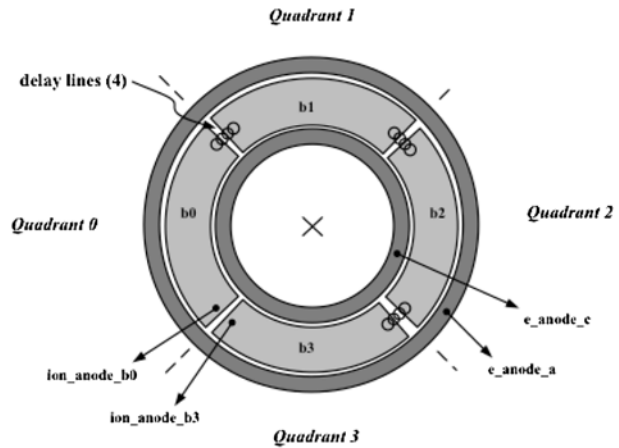


Fig. 8 Photograph of the front entrance of the TOF mass spectrometer in the test vacuum chamber. The 8 ultra-thin carbon foils are transparent and are mounted on high transmission grids. Vent holes around the grids and a general open design minimize possible acoustic damage to the foils. The entire TOF floats at 16 kV and is surrounded by the blackened aluminum ground can



foil, a fraction of them become neutral again. The ions and neutrals strike a second foil and knock off secondary electrons. These electrons are focused on the innermost radius of the MCP and constitute the second start pulse (start 2, or "c" in Fig. 7). Finally, the ions and neutrals pass through the second foil and strike the MCP in the center radius. The signal from these ions and neutrals constitutes the stop pulse (stop, or "b0" in Fig. 7). The stop anode is segmented into 4 quadrants, labeled b0, b1, b2, and b3 in Fig. 9. Delay lines are placed between anodes b0 and b1, b1 and b2, and b2 and b3. Using the delay between the signals from anodes b0 and b3, the arrival quadrant of the signal is determined. Although it is relatively crude angular information, this sectoring of the signal provides important additional background rejection when the high resolution mode is used. Since three of the four collimator quadrants are shut off in this mode, there should be minimum signal from quadrant b1, the quadrant opposite the high resolution quadrant. Tests conducted

Fig. 9 The TOF anode is divided into four sectors with delay lines between three sectors. By analyzing the signal delay between anode b0 and b3, the quadrant for the stop signal is determined



during the sensor calibration show that the ratio of the quadrant that has maximum counts to the opposite (background) quadrant is ~ 2000 . This high ratio indicates that the ion optics is behaving as designed and that the delay line detection of the ion arrival location is an effective additional background suppression technique for the interstellar neutral oxygen measurements.

3.6 TOF and Other Electronics

Electron avalanches from the back of the MCP are collected on the start 1 (a), start 2 (c), and stop (b0, b1, b2, and b3) anodes. These anodes are biased 200 V positive relative to the MCP back to accelerate the electrons from the MCP back (see Fig. 7). Four TOF ASIC chips (Paschalidis et al. 2002, 2003) combine the signals to give the ion TOF over the entire path from the first foil to the stop MCP, the half path from the second foil to the stop MCP, and between the stop anodes b0 through b3. A valid double coincidence event requires a start (two possibilities) and stop. A valid triple coincidence event requires both starts and a stop. Furthermore, a valid triple event meets the criterion that the TOF over the full 60 mm distance from the first foil to the stop MCP is equal to the sum of the TOF over the 30 mm distance from the first to the second foil and the TOF over the 30 mm distance from the second foil to the MCP. Checking that this criterion is met greatly reduces background due to random double coincidences. In particular, it eliminates events where one TOF is very near zero.

The TOF board located directly behind the MCP anode (Fig. 7) performs these logic timing determinations, monitors overall rates, and performs other housekeeping duties. Signals from this board (at the MCP high voltage) are transferred to the interface board (at sensor ground) through a pair of optical links (one for signals into the board and the other for signals out). The interface board controls TOF and PAC high voltages and is connected to the IBEX Combined Electronics Unit (CEU) through a serial port. The CEU provides conditioned, low-voltage power (± 12 V, +5 V) to the interface board, and this board distributes power that is used to create the PAC, MCP, and TOF digital voltages in the TOF HV supply (see Fig. 2).

Voltages for other parts of the IBEX-Lo sensor come from the CEU. These include the entrance subsystem voltages (high voltages for the electron repeller ($\text{CO}^- = -4.1$ kV) and the collimator ($\text{CO}^+ = +11$ kV)), optics voltages (U^+ , 4.8 kV and U^- , -2.1 kV) and

Table 2 Optics voltage settings for the IBEX-Lo sensor for the normal and special oxygen science modes

Heliospheric hydrogen science mode			
Energy Step	U+ Voltage (volts)	U– Voltage (volts)	Center energy of incident H neutrals (eV)
1	42.1	–16.8	14
2	81.2	–32.3	27
3	156	–62.2	52
4	307	–122	102
5	592	–236	197
6	1212	–482	451
7	2346	–934	908
8	4511	–1795	1903
Interstellar oxygen mode			Center energy of incident O neutrals (eV)
Jan–Feb	1035	–414	534
Oct–Nov	81	–32	33
Interstellar helium mode			Center energy of incident He neutrals (eV)
Jan–Feb	381	–152	134
Oct–Nov	41	–16	8.3

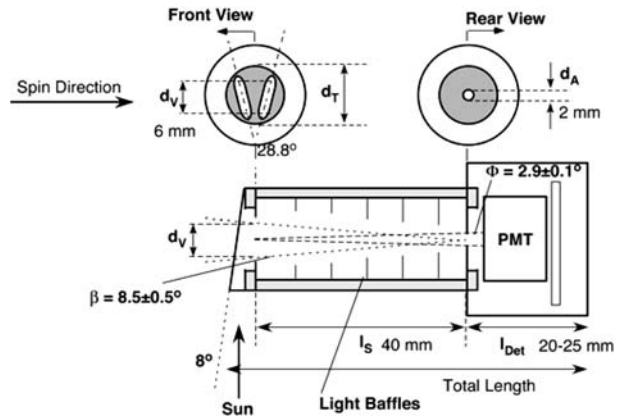
the voltage used to shut off low-resolution quadrants when in the high-resolution mode ($U_{so} = -2.5$ kV). All of these voltages are commandable to several levels, even voltages that are “fixed” at a specific voltage (e.g., U_{so}) in nominal science operations. Ion optics voltages on various electrodes are determined by the set point of the U+ and U– voltages and two high precision, high resistance resistor strings, one for each voltage. The CEU sets the five high voltages, controls their changes, and commands the TOF interface board for a particular science or engineering mode. The CEU is described in the IBEX flight segment description (Scherrer et al. 2009).

Set points for the optics voltages are shown in Table 2. For the eight energy channels in the normal (heliospheric hydrogen) science mode, the voltages fix center energies of the ESA passband that are 15% lower than the center energies of the incident neutral hydrogen. These settings assume that negative ions leave the conversion surface with 15% less energy than the incident neutrals. In the calibration, it was discovered that this energy loss is energy and mass dependent. Therefore, the highest two energy channels are not evenly logarithmically spaced from the first six channels. Also, for the special oxygen and helium modes in the spring and fall, the energy loss for oxygen off the conversion surface is much larger than that for hydrogen, so the voltages are set for correspondingly lower negative ions off the conversion surface.

3.7 Star Sensor

Accurate, absolute directional determination of interstellar neutral oxygen is critical for IBEX science closure. Therefore, a star sensor is co-aligned with the IBEX-Lo sensor to determine the absolute neutral oxygen arrival direction with respect to several stars. The star

Fig. 10 Schematic of the IBEX-Lo star sensor. The front aperture is shaped into a “v” so that as a star passes in front of the spinning aperture, a double pulse is produced in the photomultiplier tube (PMT). The time between the two pulses is used to determine the elevation angle (up/down in the figure) of a star. The azimuthal (within the spin plane) direction is determined from the center time of the two pulses and spacecraft attitude information



sensor provides data for determining positions of as many stars as possible to an accuracy of $\pm 0.1^\circ$ relative to the IBEX-Lo collimator bore sight (after ground processing).

The star sensor basic design is shown in Fig. 10, and a picture of the star sensor attached to the optics deck (with a protective cover over the aperture) is shown in Fig. 3. The star sensor operates similarly to a Sun sensor on a spinning spacecraft. It consists of an entrance aperture and collimator tube, exit pinhole, and photomultiplier tube (PMT). The entrance aperture has two slits in the shape of a “V”. As the spacecraft spins, the light curve from a star in the FOV generates two 3° wide triangular shaped peaks with full-width half-maximum separation equal to the angular aperture width. The time difference between peaks determines the elevation angle of the star with respect to the star sensor bore sight. The IBEX spin period is planned to be 4 ± 0.5 rpm. Calculations show that an integration period of 11 ms is equivalent to 1° in the spin direction. Given a FWHM of 3° for the triangular shaped peak for a star, this resolution is adequate for determining star directions within the accuracy requirements. The star sensor is sensitive to between 50 and 100 stars brighter than magnitude 2.5 in the visible part of the spectrum.

Star sensor signals are accumulated in CEU memory over multiple spins (typically ~ 64) in $720, 0.5^\circ$ bins to form a 360° histogram. The absolute reference of this histogram is the spacecraft spin pulse, which is provided by the spacecraft to the CEU. These data are processed on the ground to determine the absolute direction of the star from the azimuth location of the two peaks in the spin plane and the time separation of the two peaks.

3.8 Prototype Tests Prior to Sensor Development

Prior to the IBEX-Lo design phase, a prototype IBEX-Lo sensor was developed and tested using both ions and neutrals (Wieser 2005; Wieser et al. 2007). This prototype had the same basic geometry and design as the flight sensor except that the conversion surface was placed on the outside circumference of the prototype. Also, for initial tests, a single microchannel plate detector was used in place of the TOF mass spectrometer. Test and calibration were performed at the University of Bern MEFISTO calibration facility (Martí et al. 2001). This facility provides a calibrated neutral beam in the energy range from 10 eV to 3 keV. The same facility was used to test and calibrate the IBEX-Lo flight sensor.

The prototype design was somewhat different because one of the tests used a positive ion beam injected at the position and angle of specularly reflected negative ions off the

conversion surface. These tests verified the ion optics properties of the ESA. In particular, it verified radial focusing and azimuthal defocusing properties of the ion optics system. Positive ions were used (with the appropriate reversal of ion optics voltages) because ion beam angular width, energy spread, and flux are much better controlled than neutral beam parameters. After these tests, the aperture was replaced with a DLC conversion surface like the one used in the IBEX-Lo flight sensor, ion optics voltages were reversed, and a neutral beam was used to complete testing.

The neutral beam was produced by surface neutralization (Wieser and Wurz 2005): a 3 kV ion beam (H^+ and O^+ beams were used for the prototype testing, and H^+ , O^+ , He^+ and C^+ were used in the IBEX-Lo flight sensor calibration) with narrow (about 3 eV) energy spread was injected into the neutralizer unit (Wieser and Wurz 2005). In the neutralizer unit, the ion beam was slowed in an ion deceleration stage by retarding potentials to select a beam energy from 10 eV to a maximum of 3 keV (i.e., no deceleration of the initial beam). The decelerated ion beam was directed onto a highly polished, mono-crystalline tungsten surface at a very shallow angle (10°) where it is very efficiently neutralized. Residual ions in the resulting neutral beam were deflected away from the neutralizer exit slit using a set of electrostatic deflection plates. The neutral beam had a large energy and angle spread caused by the reflection/neutralization process. This large energy and angle spread complicates analysis of the test data. The current off the surface was calibrated prior to prototype tests (and also prior to and after the flight sensor calibration) so that absolute neutral fluxes were known to $\sim 20\text{--}30\%$.

Prototype tests using the neutral beam confirmed the energy resolution of the system, verified the ESA transmission function ($= 0.4$, approximately independent of energy), and demonstrated the overall geometric factor of the sensor. Later, the sensor was upgraded to include “fins” on the outer ESA (like the ones in Fig. 2) and to include magnets. The upgrades verified the importance of both the fins in reducing the scattered ion background and the magnets in reducing electron transmission through the ESA.

Upon completion of the tests of the upgraded prototype, the flight sensor design was developed by starting with the prototype geometry and adjusting and optimizing voltages and geometries of the electrodes. This optimization was done in an iterative process using a computer code (Wieser et al. 2008) to maximize sensor throughput and add features that simplify manufacturing and reduce the number of high voltage supplies needed to control the ion optics.

3.9 Flight Sensor Calibration and Performance

For the flight sensor, the entrance and mass analysis subsystems were tested separately. Tests of the entrance system were done to verify collimator performance including transparency, energetic particle rejection, and off axis leakage. In all of these tests, the collimator performed within the specifications. Figure 11 shows the solid angle FOV of the low-resolution quadrants of IBEX-Lo as obtained by a Monte-Carlo simulation with maximum manufacturing tolerances on the etched plates that make up the collimator. The simulated leakage over the entire accessible angle space was less than 10^{-6} of the total FOV, (i.e. two orders of magnitude better than the requirement). Combined effects of leakage through neighboring channels of the collimator and scattering off edges of the collimator plates were investigated using the collimator, a detector, and an intense Argon ion beam. An angular scan across the collimator FOV, with the ion beam intensity increased by a factor of 100 for large angles θ , is shown in Fig. 12. The observed particle rate outside the collimator FOV is typically a factor of 10 below the required suppression of 10^{-4} .

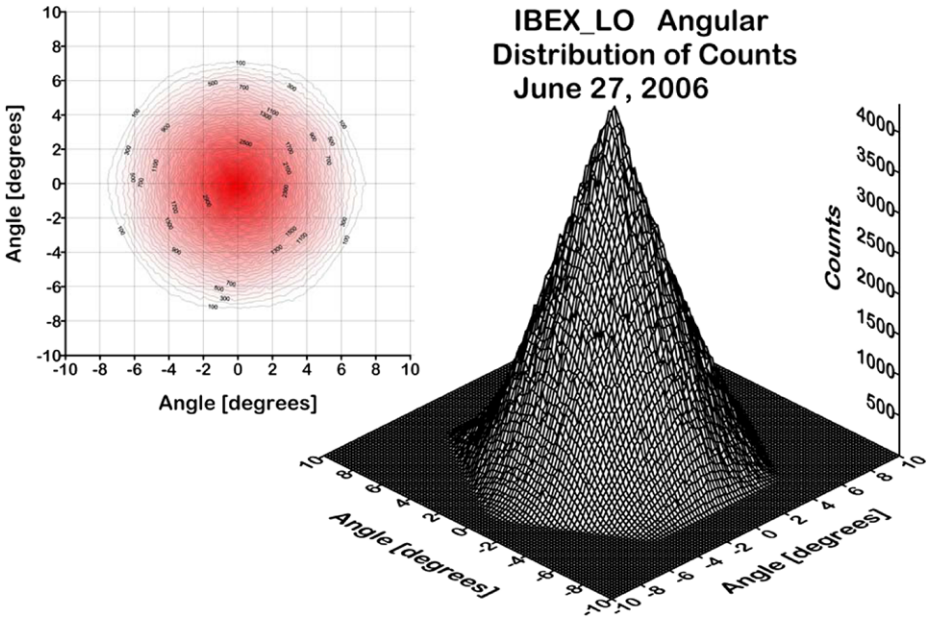
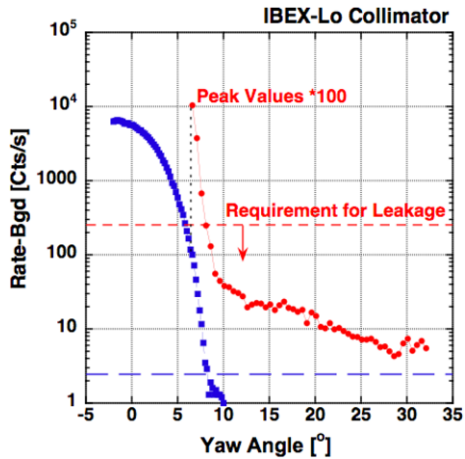


Fig. 11 Calibration results. Transmission function of high resolution sectors of the IBEX-Lo collimator. The transmission is nearly symmetric with a FWHM of $\sim 7^\circ \times 7^\circ$

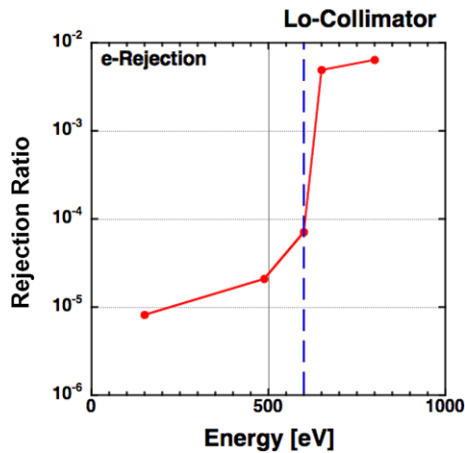
Fig. 12 On- and off-axis performance of the IBEX-Lo collimator. The on-axis profile (blue curve) shows the near-gaussian response of the collimator. The off-axis profile (red curve, note the change in scale by a factor of 100), is well below the requirement for leakage outside of $\sim 14^\circ$ yaw angle



A positive biased collimator collects plasma electrons from the environment and photo-electrons emitted from the sun-lit side of the spacecraft. In significant numbers, these electrons could be responsible for a substantial background. Thus, electron suppression, especially at low energies, is a critical requirement for the IBEX-Lo sensor. The suppression factor for electrons is shown as a function of electron energy in Fig. 13. These data are taken from tests with the IBEX-Lo entrance subsystem and an electron beam.

The mass analysis subsystem was sufficiently complicated that it required separate testing. In addition, a significant simplifying feature of the mass analysis subsystem was that

Fig. 13 Measured electron rejection properties of the IBEX-Lo collimator. With -3.1 kV on the electron rejection rings (see Fig. 2), electron fluxes below 600 eV are reduced by almost 3 orders of magnitude



voltages could be reversed and positive ions could be used to verify basic performance, mass resolution, and overall efficiency. These positive ion beam tests were performed at the University of New Hampshire. Similar to the prototype tests, positive ions have the advantage that ion beam angular width, energy spread, and flux are much better controlled than similar neutral beam parameters.

The mass analysis subsystem performed within specifications. Because singles rates and all double coincidence rates are monitored in the TOF and because the triple coincidence rate is determined from these TOF events, the absolute TOF efficiency can be determined independent of whether the TOF is tested with the sensor or tested alone. In particular, because the triple and double coincidence rates can be used to derive detector efficiencies, the IBEX-Lo TOF subsystem is fully self-calibrating, even in flight, without need to correct for any background or sensor inefficiencies. Figure 14 shows TOF double and triple coincidence efficiencies for hydrogen and oxygen as a function of MCP voltage. These tests were done during final calibration, but they confirm measurements from the University of New Hampshire ion beam tests prior to sensor assembly.

The sensor was assembled and tested in two stages. First, the ENA to ion conversion subsystem, energy analysis subsystem, and mass analysis subsystems were tested (without the entrance subsystem) using the neutral beam. These initial “pre-cal 1” tests verified basic sensor performance in a configuration similar to the prototype tests. In particular, the calibration verified that the energy subsystem had an overall throughput of 0.4, essentially independent of energy. After these first tests, the complete sensor was tested and calibrated with the neutral beams. Figures 15 and 16 show the installation of the complete IBEX-Lo sensor into the calibration vacuum chamber and the sensor as installed for the final calibration tests. Figure 15 provides a good perspective of the sensor size compared to a person. The sensor was installed in a rotation stage that was mounted on a 5-axis motion table. The rotation stage allowed tests of the azimuthal response of the sensor while the motion table was used to test the radial and radial angle response. In Fig. 16, the neutral beam source is at the left. (The ion beam that feeds this neutralizer source is in a separate beam line that enters the chamber from the left of the picture.)

Figure 17 shows sample results from the IBEX-Lo calibration. The eight peaks in Fig. 17 correspond to the 8 energy bins of the sensor and show the energy response. These data were obtained by setting the neutral beam to the center energy of a particular energy bin and scanning the sensor energy acceptance over the beam energy. The flux measured at each

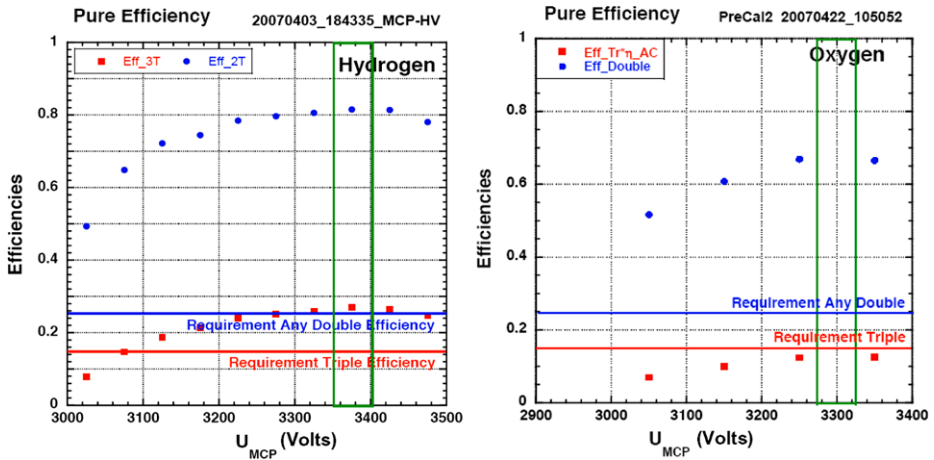


Fig. 14 TOF detection efficiencies for hydrogen (*left panel*) and oxygen (*right panel*) as a function of the MCP voltage. The MCP voltage will be set so that the detector is run in saturation mode. In this mode, the double and triple coincidence efficiencies are well above the requirements

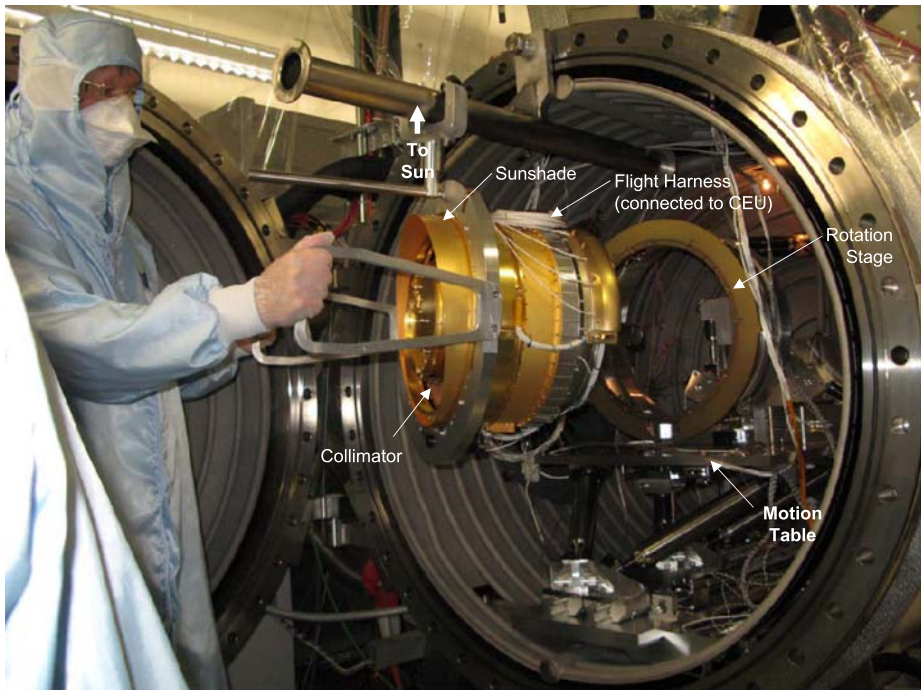


Fig. 15 Installation of the IBEX sensor into the calibration vacuum chamber at the University of Bern. The sensor is installed in a rotation stage so that the neutral beam can be directed into different parts of the collimator. The rotation stage is mounted on a motion table that allows vertical and horizontal motion to investigate sensor radial and radial angle responses

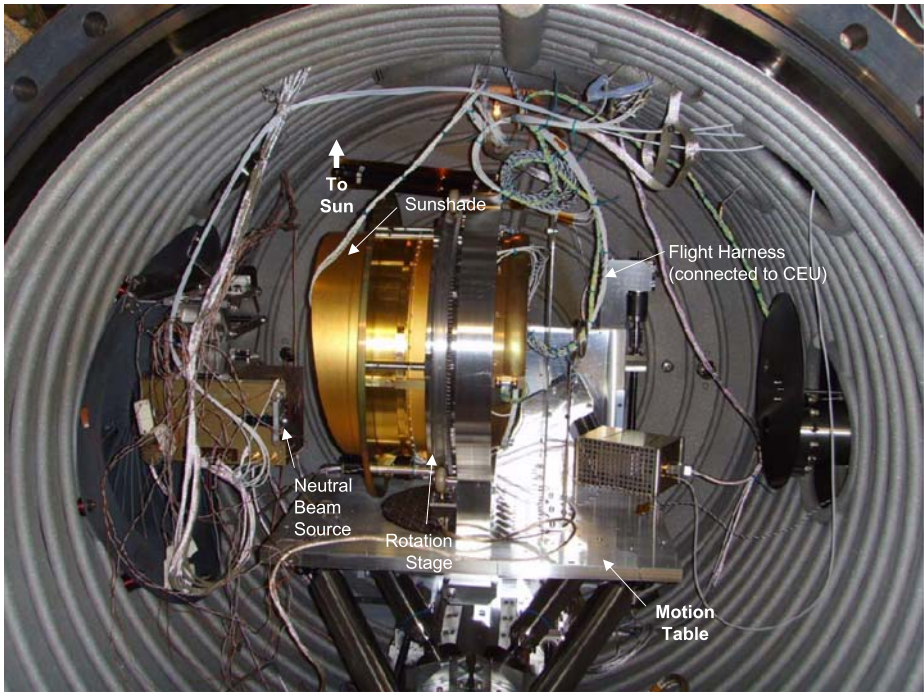


Fig. 16 IBEX-Lo installed in the calibration chamber. The neutral beam is mounted on the left and directs neutrals into the lower part of the collimator

sensor energy setting was normalized to the flux measured at the nominal center energy of the beam. Although some energy spread is due to the broad energy spread of the incident neutral beam, most of the energy spread in Fig. 17 is due to the broad $\Delta E/E$ of the energy analysis subsystem. These data were used to derive the $\Delta E/E$ of the sensor. The sensor $\Delta E/E = 0.8$ and is the combined passband of the ESA alone (which is predicted to be ~ 0.67) and the extraction system of the conversion surface. This $\Delta E/E$ is constant over the energy range.

Analysis of the calibration data indicated that the peak countrate does not occur when the sensor energy step is the same as the center energy of the beam. At low energies (below several hundred eV), this discrepancy is explained by the difficulty to produce a neutral beam with energies between ten and several hundred eV in the calibration facility. At all energies, the center energy of the beam is difficult to predict because neutrals lose energy off the tungsten neutralization surface and then lose more energy when they interact with the conversion surface in the sensor. However, measured center energies of the first 5 energy steps correspond reasonably well to the predicted energies. For the last 3 energy steps, energy loss off the IBEX-Lo conversion surface is greater than the predicted value of 15%. Figure 18 shows the energy loss of hydrogen and oxygen off the conversion surface as a function of incident neutral energy. Since voltages on the ESA were designed to pass negative ions with 15% less than the incident neutral energy, greater loss off the conversion surface translates into a higher incident neutral energy. Thus, in Table 2, the center energy of energy steps 6, 7, and 8 are separated from one another and from lower energy steps by greater than a logarithmic spacing (but still without any gaps). For oxygen, energy losses off the conversion surface are

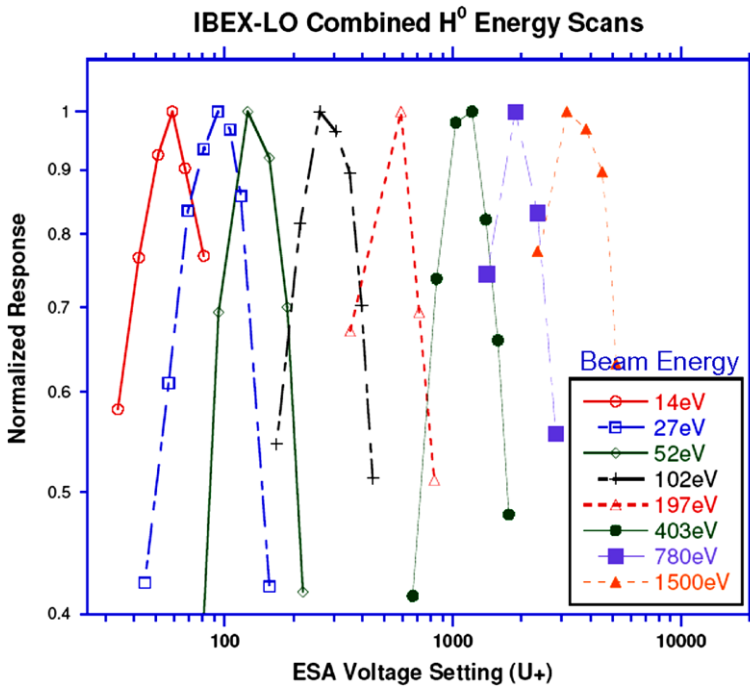


Fig. 17 Measured hydrogen fluxes in each of the 8 energy bins as a function of the ESA voltage. In this test, the neutral beam energy was fixed at the values shown in the legend. Energy bins have significant overlap with a $\Delta E/E$ of 0.8

Fig. 18 Negative ion energy loss as a function of neutral beam energy. Negative ions lose energy off the conversion surface and this energy loss is species and beam energy dependent. The ESA bandpasses are designed to account for this energy loss

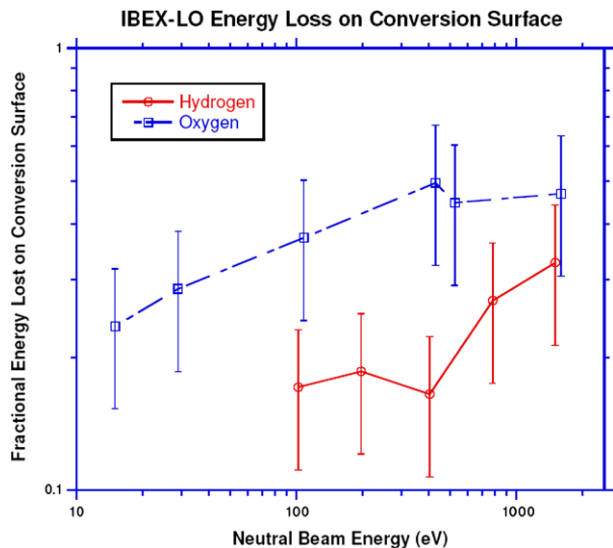
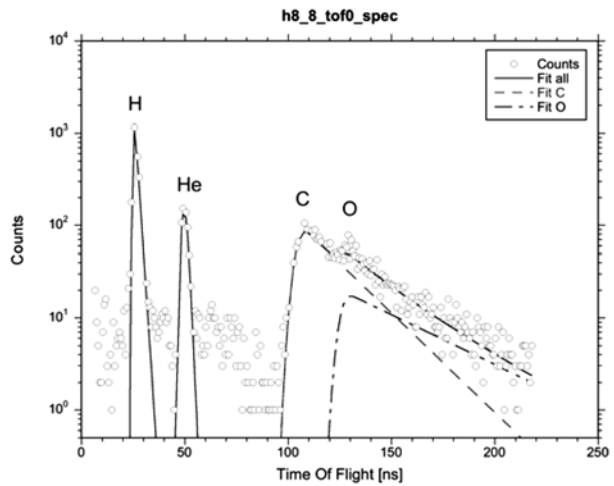


Fig. 19 TOF mass spectrum from the IBEX-Lo flight sensor. A neutral helium beam was used in this test. The masses observed include helium (converted to He⁻ at the conversion surface) and H, C, and O sputtered from the conversion surface and from the breakup of water on the conversion surface



even higher as are the corresponding center energies of incident oxygen neutrals. However, the science objectives of the sensor focus on detection of heliospheric hydrogen neutrals. Thus, for normal science operations, ESA voltages and corresponding energy steps are designed to produce a quasi-logarithmically spaced set of energy channels for hydrogen from 10 eV to ~ 2 keV. The energy steps for oxygen are determined from these voltages, but the voltages are set for hydrogen. For the special operations to detect interstellar neutral oxygen in October and January, the sensor energy step is fixed for the center energy of arriving oxygen neutrals. These voltages, using the calibrated higher energy loss off the conversion surface, are shown in Table 2.

Figure 19 shows a mass spectrum measured by the IBEX-Lo sensor. This figure illustrates important properties of low energy neutral detection using the conversion surface ionization technique. For this test, a 1.5 keV neutral helium beam was directed into the IBEX-Lo sensor. The sensor was set to detect neutrals centered at 1.5 keV, the same energy as the beam. There are several mass peaks in the spectrum. The H, C, and O mass peaks are caused by recoil sputtering of negative ions from the DLC conversion surface by the neutral helium beam. Only the mass peak identified as He is produced by true conversion of neutral helium into He⁻ on the conversion surface. Unlike neutrals with high electron affinity, He⁻ is not stable and survives only because of the relatively short flight time from the conversion surface to the TOF entrance (Wurz et al. 2008a). The ionization efficiency for helium is very low ($\sim 10^{-5}$), thus the peak is considerably lower than the recoil sputtered products. For other neutral beams with high electron affinity (i.e., neutral hydrogen or oxygen), nearly 100% of the signal observed at beam energies ~ 1 keV is true conversion to a negative ion. However, all neutrals produce sputtered products at low energies (~ 10 's of eV and greater). Thus, analysis of the IBEX-Lo signal at low energies requires knowledge of the flux of high energy (~ 1 keV) neutrals on the surface so that low-energy sputtered products from these neutrals can be subtracted from the observed total flux.

Table 3 shows sensor geometric factors for each energy step for double and triple coincidence hydrogen. These factors were determined from the calibration and include the sensor $\Delta E/E$, collimator solid angle FOV, all of the efficiencies of transmission through the collimator, internal grids transmission, effects of the spokes that separate each azimuthal quadrant, the energy dependent conversion efficiency, and TOF efficiencies.

Table 3 $G\Delta E/E$ for the IBEX-Lo sensor, determined from calibration

Energy Step	Center Energy (eV)	$G\Delta E/E$ for any double coincidence hydrogen ($\text{cm}^2 \text{sr eV/eV}$)	$G\Delta E/E$ for triple coincidence hydrogen ($\text{cm}^2 \text{sr eV/eV}$)
1	14	7.5×10^{-5}	2.7×10^{-5}
2	27	1.5×10^{-4}	5.3×10^{-5}
3	52	2.2×10^{-4}	8.1×10^{-5}
4	102	2.5×10^{-4}	9.1×10^{-5}
5	197	2.5×10^{-4}	9.0×10^{-5}
6	451	2.9×10^{-4}	1.0×10^{-4}
7	908	5.4×10^{-4}	1.9×10^{-4}
8	1903	7.6×10^{-4}	2.7×10^{-4}

Background suppression is a critical element of the IBEX-Lo design. Suppression of any background that can masquerade as signal neutrals is particularly important because the heliospheric neutral source strength is low. In a separate paper in this volume (Wurz et al. 2009), background sources are discussed in detail. In nearly all instances, background consists of positive ions produced at or behind the collimator exit that are accelerated to high voltage by the collimator positive voltage. This background flux depends on the residual gas pressure in this part of the sensor. To reduce this gas pressure, the sensor has significant vent paths that bypass this critical region (see Fig. 2), sensor electronics are vented separately from sensor optics, there are no vent paths to the spacecraft interior, and materials in the optics path were carefully chosen for their low outgassing properties. Based on expected on-orbit electron, ion, and photon fluxes that produce background, a residual gas pressure of $\sim 10^{-8}$ – 10^{-7} mbar is needed to keep signal to noise > 10 over the full energy range of the sensor.

Estimating residual gas pressure in the region behind the collimator is very difficult. The internal pressure depends strongly on the pumping speed of the sensor, which is determined by the ratio of interior to exterior gas pressures and the amount of pumping area available.

Because the sensor internal pressure drives most of the important background levels, this pressure was measured and compared to the pressure inside the calibration vacuum chamber. The internal pressure was measured using a nude ion gauge installed in the access port at the bottom center of the sensor (see Fig. 2). Because this location is deep inside the sensor, the pressure in this region is probably higher there than in the region just in back of the collimator. Table 4 shows results of this pressure test. The pressure was measured as the vacuum chamber pressure was decreasing by over an order of magnitude over a few hours. The internal to external pressure ratio is only a factor of ~ 2 , presumably because of the extensive measures used to vent the sensor. It is doubtful that this internal to external pressure ratio will remain a factor of two over many more orders of magnitude in pressure. However, these results are encouraging for on-orbit performance, where external pressures are expected to be 10^{-10} – 10^{-14} mbar. With these low pressures, the pressure in the critical region behind the collimator is likely to be $\ll 10^{-8}$ mbar and the background will be correspondingly low.

3.10 Sensor Operation

IBEX-Lo sensor operations on orbit are relatively simple. After initial on-orbit checkout and high voltage turn-on, the sensor operates in a single science mode during most spacecraft

Table 4 Internal sensor and external vacuum chamber pressures measured during the IBEX-Lo calibration

External (vacuum chamber) pressure (mbar)	Internal (sensor) pressure (mbar)	Ratio internal/external pressure
1.2×10^{-6}	2.5×10^{-6}	2.1
6.0×10^{-7}	1.4×10^{-7}	2.3
1.6×10^{-7}	3.8×10^{-7}	2.4

Table 5

Product	Bits per second (bps)	Comments
Quaternions	57	Spacecraft attitude
Payload	12	Sensor housekeeping
IBEX-Hi total	98	Direct events and histograms
IBEX-Lo total	115	Direct events and histograms
IBEX-Lo Telemetry Detail		
Direct events	95	About 3 events per second
H histogram	7	Various start/stop rates and additional monitor rates
O histogram	7	
Star sensor	6	Collected with 0.5° resolution

orbits. At low altitudes (< 10 Earth radii, R_E), the sensor is switched from science mode to a standby mode. In this mode, high voltages are turned down or off to eliminate high countrates in the Earth's radiation belts. Since science operations are performed above this altitude, there is no loss of science in these standard operations.

In science mode, the sensor is set at a fixed energy step for 2 spins, so that the entire energy range is sampled in 16 spins. These measurements are repeated without interruption over the entire science operations part of the spacecraft orbit.

Twice per year, the sensor is switched into a special interstellar neutral oxygen and helium mode in the science operations part of the spacecraft orbit. These times are shown in Fig. 1 and this mode is described in more detail in Möbius et al. (2009). During the fall interstellar neutral observing period, only oxygen is observed (helium is below the energy range of the sensor). In the part of the spacecraft spin when the IBEX-Lo sensor is viewing $\pm 30^\circ$ around the ecliptic, the standard 2-spin energy step sequence is interrupted and the sensor is set at a fixed energy corresponding to the expected energy of interstellar neutral oxygen.

In the spring interstellar neutral observing period, there is a similar interruption of the standard 2-spin energy stepping sequence. This time, low resolution sectors are electrostatically switched off in the region $\pm 30^\circ$ around the ecliptic and the sensor is set at a fixed energy corresponding to the expected energy of the interstellar neutral oxygen. This sequence is repeated for 7 spins. Every 8th spin, the sensor is set at a fixed energy corresponding to the expected energy of interstellar neutral helium.

3.11 Data Products

Regardless of science mode, data products and telemetry from the IBEX-Lo sensor are the same. Table 5 shows the data products that are accumulated over 64 spins (about 16 min)

and transmitted to ground during spacecraft perigee passes. The telemetry budget allows an average of 282 bps of payload telemetry (115 bps for IBEX-Lo) for most of the 8-day orbit.

Although IBEX-Lo is a triple coincidence TOF mass spectrometer, the triple coincidence is composed of double coincidence measurements. Therefore, considerably more information at higher sensitivity is available from the sensor. In particular, there are 4 double coincidence times of flight available, TOF 0, 1, 2, and 3. TOF0 is the time between the first start and the stop signals, TOF1 between the first start and the second start, TOF2 between the second start and the stop, and TOF3 is the delay line signal. TOF3 (anode 3) determines the quadrant where the stop signal originated. Each TOF is determined separately and encoded to 11 bits (0.16 ns resolution). A triple event has all 4 TOFs valid and a “golden” triple satisfies the following equation:

$$\text{Checksum} = \text{TOF0} + \text{TOF3} - \text{TOF2} - \text{TOF1} \sim 0. \quad (2)$$

The golden triples are the most interesting events because they represent the best, lowest noise signal. A full description of these events is available for transmission to ground provided the event rate is ~ 1 event/second (which is about a factor of 10 higher than the current expected rate for heliospheric neutrals). Consistent with the primary science objectives, the IBEX CEU must avoid using all of the telemetry allocation on a bright source (like the magnetosphere) and to give priority to the heliospheric measurements (which are distributed somewhat evenly over the spin). This prioritization is done in the CEU, using an algorithm that distributes the number of golden events allowed approximately uniformly over the sky. The essential component of the algorithm is that direct events are collected over an interval that is short enough that the heliosphere contributes only a count or two in any sky bin, and these are all sent to ground. Anomalously bright regions (e.g., the magnetosphere) will saturate and are counted in histograms, but all direct events from these regions are not telemetered.

Using these data, the number of triple events that could not be included in the telemetry can be reconstructed. In this manner, the actual strength of bright sources such as the magnetosphere or possibly a planetary source (e.g., Jupiter) can be determined.

4 Summary

The IBEX-Lo sensor is a single pixel, large geometric factor camera. It detects 10 eV to 2 keV heliospheric neutral hydrogen in 8, rather broad energy bands. The sensor uses surface conversion to convert neutrals into negative ions and then accelerates the ions so that they can be deflected away from UV background and can be analyzed with higher efficiency. The sensor uses a triple coincidence TOF mass spectrometer to distinguish hydrogen, oxygen, and helium from the heliosphere and from the interplanetary medium. The sensor has undergone significant test and calibration that have demonstrated that it meets requirements for the IBEX mission. Together with the IBEX-Hi sensor, this sensor will achieve the science objectives of the mission.

Acknowledgements The IBEX-Lo sensor is the result of efforts from a large number of scientists and engineers located at many institutions around the world. From conceptual design to final cross-calibration, this sensor has been a collaborative effort. All who contributed to this sensor share in its success. The success of this sensor would not be possible without the strong support of the IBEX project. This support went well beyond standard contractual and financial support and included creative solutions to procurement, processing, and testing issues that occurred during the course of the design, development, and test of the sensor.

References

- S.A. Fuselier, E.S. Claffin, S.B. Mende, C.W. Carlson, T.E. Moore, Combined in situ and remote sensing of ionospheric ion outflow. *Geophys. Res. Lett.* **33**, L04103 (2006). doi:[10.1029/2005GL024055](https://doi.org/10.1029/2005GL024055)
- A. Galli, P. Wurz, S. Barabash, A. Grigoriev, R. Lundin, Y. Futaana, H. Gunell, M. Holström, E.C. Roelof, C.C. Curtis, K.C. Hsieh, A. Fedorov, D. Winningham, R.A. Fram, R. Cerulli-Irelli, P. Bochsler, N. Krupp, J. Woch, M. Fraenz, Direct measurements of energetic neutral hydrogen in the interplanetary medium. *Astrophys. J.* **644**, 1317 (2006).
- A.G. Ghielmetti, E.G. Shelley, S.A. Fuselier, F. Herrero, M.F. Smith, P. Wurz, P. Bochsler, T. Stephen, Mass spectrograph for imaging low energy neutral atoms, in *Instrumentation for Magnetospheric Imaging II*, ed. by S. Chakrabarti, Proc. SPIE 2008, pp. 105–112, 1993; *Opt. Eng.* **33**, 362 (1994)
- Gruntman, Magnetospheric imaging (1993)
- M. Gruntman, E.C. Roelof, D.G. Mitchell, H.J. Fahr, H.O. Funsten, D.J. McComas, Energetic neutral atom imaging of the heliospheric boundary region. *J. Geophys. Res.* **106**, 15767 (2001)
- S. Jans, P. Wurz, R. Schletti, T. Fröhlich, E. Hertzberg, S. Fuselier, Negative ion production by surface ionization using aluminum-nitride surfaces. *J. Appl. Phys.* **85**, 2587 (2000)
- A. Marti, R. Schletti, P. Wurz, P. Bochsler, Calibration facility for solar wind plasma instruments. *Rev. Sci. Instrum.* **72**, 1354 (2001)
- D.J. McComas, P. Valek, J.L. Burch, C. Pollock, R.M. Skoug, M.F. Thomsen, Filling and emptying of the plasma sheet: Remote observations with 1–70 keV energetic neutral atoms. *Geophys. Res. Lett.* **29**, 2079 (2002). doi:[10.1029/2002GL016153](https://doi.org/10.1029/2002GL016153)
- D.J. McComas et al., The interstellar boundary explorer (IBEX), in *Physics of the Outer Heliosphere, Third Annual IGPP Conference*, ed. by V. Florinski, N.V. Pogorelov, G.P. Zank, AIP CP719 (2004), p. 162
- D.J. McComas et al., *Space Sci. Rev.* (2009, this issue)
- H. Moestue, The electric field and geometrical factor of an annular curved plate electrostatic analyzer. *Rev. Sci. Instrum.* **44**, 1709 (1973)
- T.E. Moore, D.J. Chornay, M.R. Collier, F.A. Herrero, J. Johnson, M.A. Johnson, J.W. Keller, J.F. Laudaudio, J.F. Lobell, K.W. Ogilvie, P. Rozmarynowsky, S.A. Fuselier, A.G. Ghielmetti, E. Hertzberg, D.C. Hamilton, R. Lundgren, P. Wilson, P. Walpole, T.M. Stephen, B.L. Peko, B. Zyl, P. Wurz, J.M. Quinn, G.R. Wilson, The low-energy neutral atom imager for IMAGE, in *The IMAGE Mission*, ed. by J.L. Burch. (Kluwer, Dordrecht, 2000). *Space Sci. Rev.* **91** (2000), pp. 155–195
- E. Möbius, D. Hovestadt, B. Klecker, L.M. Kistler, M.A. Popecki, K.N. Crocker, F. Gliem, M. Granoff, S. Turco, A. Anderson, H. Arbinger, S. Battell, J. Cravens, P. Demain, J. Distelbrink, I. Dors, P. Dunphy, J. Gaidos, J. Googins, A. Harasim, R. Hayes, G. Humphrey, H. Kästle, E. Küneth, J. Lavoisier, E.J. Lund, R. Miller, G. Murphy, E. Pfeffermann, K.-U. Reiche, E. Sartori, J. Schimpfle, E. Seidenschwang, M. Shappirio, K. Stöckner, S.C. Taylor, M. Vosbury, W. Wiewesiek, V. Ye, The solar energetic particle ionic charge analyzer (SEPICA) and the data processing unit (S3DPU) for SWICS, SWIMS and SEPICA. *Space Sci. Rev.* **86**, 447 (1998a)
- E. Möbius, L.M. Kistler, M. Popecki, K. Crocker, M. Granoff, Y. Jiang, E. Sartori, V. Ye, H. Rème, J.A. Sauvaud, A. Cros, C. Aoustin, T. Camus, J.L. Médale, J. Rouzaud, C.W. Carlson, J.P. McFadden, D.W. Curtis, H. Heeterks, J. Croyle, C. Ingraham, E.G. Shelley, D. Klumpar, E. Hertzberg, B. Klecker, M. Ertl, F. Eberl, H. Kästle, E. Küneth, P. Laeverenz, E. Seidenschwang, G.K. Parks, M. McCarthy, A. Korth, B. Gräwe, H. Balsiger, U. Schwab, M. Steinacher, The 3-D plasma distribution function analyzers with time-of-flight mass discrimination for CLUSTER, FAST and Equator-S, measurement techniques in space plasmas, ed. by R. Pfaff, J. Borowski, D. Young. *Geophys. Monograph* 102 (1998b), p. 243
- E. Möbius, S. Fuselier, M. Granoff, E. Hertzberg, B. King, H. Kucharek, S. Livi, S. Longworth, N. Paschalidis, L. Saul, J. Scheer, C. Schlemm, M. Wieser, P. Wurz, Time-of-flight detector system of the IBEX-Lo sensor with low background performance for heliospheric ENA detection, Proc. of the 30th Int. Cosmic Ray Conf., on CD (2007)
- E. Möbius et al., *Space Sci. Rev.* (2009, this issue)
- N.P. Paschalidis et al., A CMOS time of flight system on a chip for spacecraft instrumentation. *IEEE Trans. Nucl. Sci.* **49**, 1156–1163 (2002)
- N.P. Paschalidis, Advanced system on a chip microelectronics for spacecraft and science instruments. *Acta Astronaut.* **52**(2–6), 411–420 (2003)
- Pollock et al., Medium energy neutral atom (MENA) imager for the IMAGE mission, in *The IMAGE Mission*, ed. by J.L. Burch (Kluwer, Dordrecht, 2000), pp. 113–154
- J.A. Scheer, M. Wieser, P. Wurz, P. Bochsler, E. Hertzberg, S.A. Fuselier, F.A. Koeck, R.J. Nemanich, M. Schleberger, High negative ion yield from light molecule scattering. *Nucl. Instr. Meth. Phys. Res. B* **230**(1–4), 330–339 (2005). doi:[10.1016/j.nimb.2004.12.063](https://doi.org/10.1016/j.nimb.2004.12.063)
- J.A. Scheer, M. Wieser, P. Wurz, P. Bochsler, E. Hertzberg, S.A. Fuselier, F.A. Koeck, R.J. Nemanich, M. Schleberger, Conversion surfaces for neutral particle imaging detectors. *Adv. Space Res.* **38**(4), 664–671 (2006)

- J. Scheer, P. Wahlström, P. Wurz, E. Hertzberg, S. Fuselier, Scattering properties of hydrogen and oxygen on artificial diamond surfaces using in space flight, Nucl. Instr. Meth. B (2008, in preparation)
- J. Scherrer et al., Space Sci. Rev. (2009, this issue)
- X. Shelley et al., The toroidal imaging mass-angle spectrography (TIMSA) for the polar mission. Space Sci. Rev. **71**, 497 (1995)
- P. Wahlström, J. Scheer, P. Wurz, E. Hertzberg, S. Fuselier, Calibration of charge state conversion surfaces for neutral particle detectors. J. Appl. Phys. **104**, 034503-1–034503-6 (2008). doi:[10.1063/1.2957064](https://doi.org/10.1063/1.2957064)
- M. Wieser, Detection of energetic neutral atoms and its application to heliospheric science. PhD Thesis, University of Bern (2005)
- M. Wieser, P. Wurz, Production of a 10 eV–1000 eV neutral particle beam using surface neutralization. Meas. Sci. Technol. **16**, 2511–2516 (2005)
- M. Wieser, P. Wurz, R.J. Nemanich, S.A. Fuselier, Secondary electron emission of chemical-vapor-deposited diamond by impact of slow H^+ , D^+ , H_2^+ , C^+ , O^+ , and O_2^+ ions. J. Appl. Phys. **98**, 034906 (2005). doi:[10.1063/1.1996855](https://doi.org/10.1063/1.1996855)
- M. Wieser, P. Wurz, E. Möbius, S.A. Fuselier, E. Hertzberg, D.J. McComas, The ion-optical prototype of the low energy neutral atom sensor of the interstellar boundary explorer mission (IBEX). Rev. Sci. Instr. **78**, 124502-1–124502-14 (2007)
- M. Wieser, P. Wurz, E. Möbius, S.A. Fuselier, E. Hertzberg, D.J. McComas, Development of the low energy neutral atom sensor of the Interstellar Boundary Explorer Mission (IBEX). Rev. Sci. Instrum. (2008, in press)
- P. Wurz, Detection of energetic neutral particles, in *The Outer Heliosphere: Beyond the Planets*, ed. by K. Scherer, H. Fichtner, E. Marsch (Copernicus Gesellschaft e.V., Katlenburg-Lindau, 2000), pp. 251–288
- P. Wurz, P. Bochsler, A.G. Ghielmetti, E.G. Shelley, F. Herrero, M.F. Smith, Concept for the Hi-LITE neutral atom imaging instrument, in ed. by P. Varga and G. Betz, *Proceedings of Symposium on Surface Science*, Kaprun, Austria (1993), p. 225
- P. Wurz, R. Schletti, M.R. Aellig, Hydrogen and oxygen negative ion production by surface ionization using diamond surfaces. Surf. Sci. **373**, 56–66 (1997)
- P. Wurz et al., Formation of negative ions by scattering from a diamond (111) surface, in *Proc. of the Week of Doctoral Students*, ed. by J. Safrankova, A. Koruka (Charles University, Prague, 1998), p. 257
- P. Wurz, J. Scheer, M. Wieser, Particle scattering off surfaces: application in space science. e-J. Surf. Sci. Nanotechnol., **4**, 394–400 (2006)
- P. Wurz, L. Saul, J.A. Scheer, E. Möbius, H. Kucharek, S.A. Fuselier, Negative helium generation upon surface scattering: Application in space science. J. Appl. Phys. **103**, 054905 (2008a)
- P. Wurz, A. Galli, S. Barabash, A. Grigoriev, Energetic neutral atoms from the heliosheath. Astrophys. J. **683**, 248 (2008b) doi:[10.1086/589854](https://doi.org/10.1086/589854)
- P. Wurz, Space Sci. Rev. (2009, this issue)